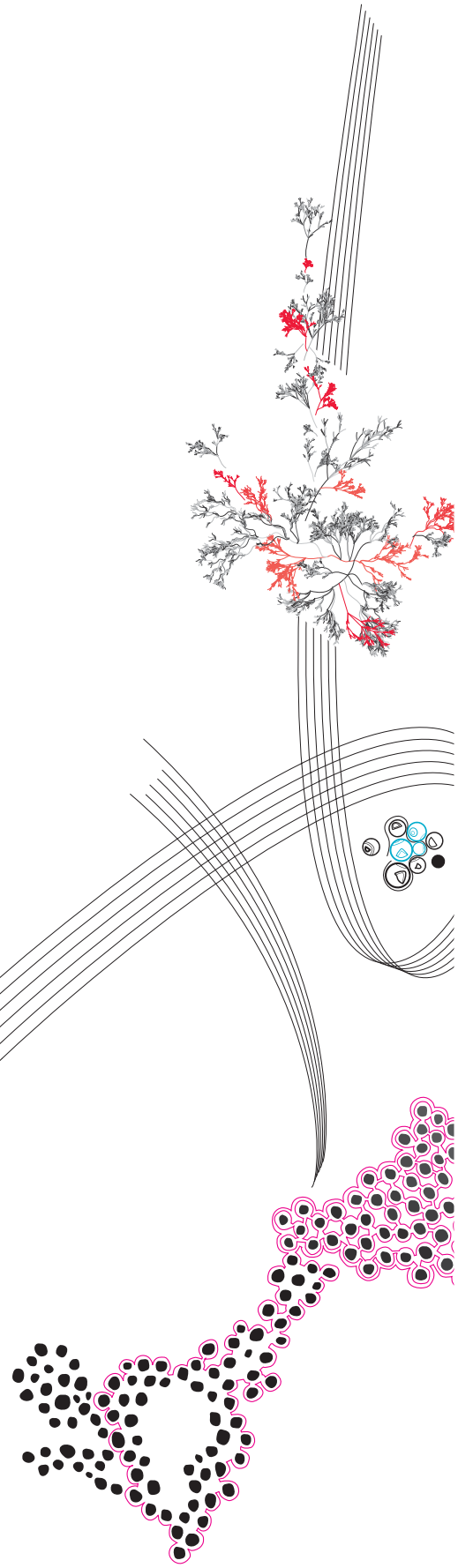

MSc Civil Engineering & Management
(River & Coastal Engineering)

Near-bed orbital velocities at the toe of a Living Dike: Insights from Deltaflume experiments and SWASH numerical modeling

D. de Graaf

Supervisor:
Dr. Ir. J.J. van der Werf (University of Twente)

Daily advisor:
Ir. J.R.M. Muller (University of Twente)
Ir. E.E. Sirks (Witteveen+Bos)

February, 2025

Department of Engineering Technology,
Faculty of Civil Engineering,
Water Engineering and Management

UNIVERSITY OF TWENTE.

LIVING DIKES

Witteveen + Bos

Preface

This thesis finishes up my Master of Science in Civil Engineering and Management with the specialization River and Coastal Engineering at the University of Twente. This project is executed in collaboration with Witteveen+Bos, Deltares and the University of Twente, within the Living Dikes research project to obtain more knowledge about the dynamics of saltmarshes under storm conditions. This thesis in particular concerns exploring the near-bed orbital velocity conditions at the toe of a dike fronted with a saltmarsh. During this project I learned a lot about the effect of saltmarshes on wave characteristics, data analysis of flume measurements and numerical modeling.

To start with, I want to thank my supervisors for the guidance during this project. From Witteveen+Bos, I want to thank Emma Sirks. Emma helped me around the project concerning critical thinking and feedback of the results and providing with good practical programming and project management tips. Emma also showed me how commercial engineering firms operate and work, providing me with valuable lessons for the future.

I also want to thank Jos Muller from the University of Twente for his guidance. Jos conducted the measurements for the Deltaflume experiments, and assisted me with the analysis and understanding of the results. Jos also provided me with a good critical perspective of the results and valuable discussion sessions.

Jebbe van der Werf from the University of Twente also provided me with good feedback and discussion sessions concerning the results of the research. I want to thank Jebbe for his critical thinking, quick responses and thinking along with the project.

This research would not have been possible without the Living Dikes project and the Deltaflume tests that are conducted at Deltares. I want to thank Deltares for the possibility to work on this project and the possibility to visit and observe the experiments that are conducted in the Deltaflume. Next to that I want to thank all the people that collaborated on the Deltaflume measurements, without them this thesis would not have been possible.

To finish up, I want to thank all my friends, family and my girlfriend for supporting me throughout my student career, who supported me and distracted me from the exams and deadlines.

With this thesis, I hope the design of dikes fronted with saltmarshes can be optimized and the near-bed velocities at the toe of a dike fronted with a saltmarsh are understood better.

Enjoy reading this thesis!

Dennis de Graaf

Utrecht, February 2025

Abstract

The rapidly changing climate influencing flood protection is one of the major challenges society is facing. The coming century, accelerated sea level rise, increase in frequency of storms is expected (Arias et al., 2021). These climate driven hazards increase hydrodynamic loads on coastal structures. A potential remedy for improving flood safety worldwide are nature-based flood defenses, where the ability of saltmarshes to attenuate waves during storm conditions can be used for strengthening coastal flood defenses. Saltmarshes can erode under storm conditions, although a lot of research is conducted about saltmarsh dynamics, the erosion mechanics at the transition point between a dike and a saltmarsh are not well understood. This study explores how the near-bed orbital velocities act at the transition point between the saltmarsh and a dike for varying storm conditions.

Theoretical methods to obtain the near-bed orbital velocities at the toe of a dike are tested and compared to results of unique full scale experiments carried out at the Deltaflume, Deltares. In the Deltaflume, full scale tests have been conducted to gain insights in the dynamics on a saltmarsh during storm conditions. This study investigates Acoustic Doppler Velocimeter measurements taken at the toe of a dike, along with offshore and near-toe wave height measurements. The study incorporates the data preparation and filtering to obtain reliable results from the measurement devices. The obtained velocity data ($\hat{u}_{2\%}$ and $\hat{u}_{33\%}$) are obtained for all tested storm conditions in the Deltaflume and compared with theoretical methods. A substantial decrease in near-bed orbital velocities is observed when comparing fully vegetated experiments to those without vegetation and no erosion is present at the transition point. The study also emphasizes the impact of frequency-dependent dissipation in vegetation on near-bed orbital velocities.

Additionally, near-bed velocity and wave height measurements are used to calibrate a 2DV SWASH numerical model, extending the dataset and providing deeper insight into near-bed orbital velocities at the toe of a dike fronted with a saltmarsh. The model employs a multi-layer approach to achieve the most realistic numerical simulations possible for both wave attenuation and near-bed orbital velocities. The modeling is conducted for both bare as for vegetated saltmarshes using well known approximations for bed roughness and vegetation drag. Insights include the changing near-bed orbital velocities due to a change in velocity profile due to increasing water levels. The main governing parameter that maximizes near-bed orbital velocities is the $\frac{H_{m0}}{h_k}$ ratio, which is extensively modeled in this study without vegetation present. The numerical model is also used to evaluate the impact of dike slopes on near-bed orbital velocities at the dike toe, providing insight into the optimal dike slope under varying conditions. However, it does not offer a precise analysis of the governing hydrodynamics.

This study shows that saltmarshes can significantly reduce near-bed orbital velocities at the toe of a dike. For further research, enhancing the accuracy of the numerical model is recommended and additional simulations can enhance the understanding of the near-bed orbital velocities at the toe of a dike. Vegetation modeling could be more effective with additional time for calibration, potentially using an alternative numerical model. The dataset obtained from the Deltaflume serves as an excellent resource for calibrating numerical models.

Table of Contents

List of Figures

List of Tables

List of parameters

Parameter	Description	Units
α_i	Phase, between 0 and 2π	[rad]
$\hat{u}$	Near-bed orbital velocity in x-direction	[m/s]
$\hat{u}_{2\%}$	Highest 2% near-bed orbital velocity in x-direction	[m/s]
$\hat{u}_{33\%}$	Highest 33% near-bed orbital velocity in x-direction	[m/s]
ν_k	Kinematic viscosity	[m²/s]
ω	Angular frequency	[rad/s]
ρ	Density of water	[kg/m³]
σ	Spectral width parameter (JONSWAP shape parameter)	[-]
τ_b	Bed shear stress	[N/m²]
a	Amplitude of a wave	[m]
C	Courant number (numerical stability criterion)	[-]
C_d	Drag coefficient	[-]
C_f	Friction coefficient	[-]
d	Water depth	[m]
f	Frequency of a wave	[Hz]
f	Friction factor in bed shear stress	[-]
g	Gravitational acceleration	[m/s²]
h	Water depth	[m]
H_{m0}	Significant wave height based on zeroth spectral moment	[m]
h_k	Water depth above salt marsh	[m]
H_s	Significant wave height	[m]
h_t	Water depth above toe (structure/bed feature)	[m]
k	Wave number	[1/m]
L	Wave length	[m]
$L_{m-1,0}$	Mean wave length based on spectral moments m_{-1} and m_0	[m]
m_0	Zeroth order moment of the wave spectrum	[m²]
n	Manning roughness coefficient	$[s/m^{1/3}]$
P	Wave power per unit crest length	[W/m]
Re_v	Reynolds number in vegetation flow	[-]
S	Power spectral density of waves	[W/m²/Hz]
S_d	Stem diameter	[m]
s_{op}	Operational wave steepness	[-]
SNR	Signal-to-Noise Ratio	[-]
t	Time	[s]
$T_{m-1,0}$	Mean wave period based on spectral moments m_{-1} and m_0	[s]
T_p	Spectral peak period (period of dominant waves)	[s]
T_z	Zero-crossing wave period	[s]
u	Flow velocity	[m/s]
U	$u_{2\%}$ value in bed shear stress formula	[m/s]
U_{max}	Peak velocity by linear wave theory	[m/s]
U_{rms}	Root mean square velocity	[m/s]
x	Numerical grid location	[m]
z	Water depth in numerical model	[m]
z	Bed level	[m]

1 Introduction

1.1 Problem context

One of the major challenges society is facing in the near future, is ensuring flood protection in a rapidly changing climate. The coming century, the IPCC (Intergovernmental Panel on Climate Change) expects accelerated sea level rise (SLR), an increase in the frequency of storms and an increase in extreme droughts and heats (Arias et al., 2021). These climate changes influence the assessment and management of the current flood protection and adds another magnitude of uncertainty, making future flood protection measures challenging. In order to address these challenges, flexible solutions need to be developed to adapt to or mitigate the impacts of climate change in flood protection. Primarily, coastal areas are vulnerable to an increased storminess and SLR. Oppenheimer et al. (2022) describes multiple strategies to adapt to climate change (see Figure 1.1). Common practice for coastal protection is the use of hard structures (e.g. dikes covered with asphalt or rock revetments). Due to the static nature of these hard structures, they require constant maintenance and heightening to withstand the impacts of SLR increase in storminess. Additionally, the ongoing maintenance and heightening is very costly and disturbing for the surrounding area. Advancing and retreating measures (Figure 1.1b & d, respectively) are often not a viable option due to the extensive development of urban or agricultural areas (Singh, 2020).

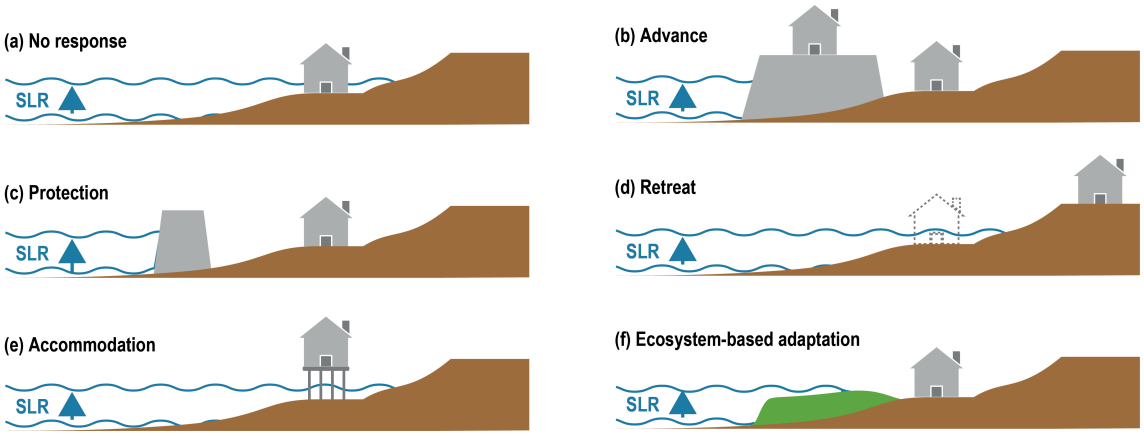

FIGURE 1.1: Different types of responses to coastal risk and SLR (Oppenheimer et al., 2022)

An innovative response to climate change is ecosystem-based adaptation (Figure 1.1f). The combination of hard structures and ecosystem-based adaptation measures fall under Nature-based Solutions (NbS) in practice (de Vriend et al., 2014). NbS encompass a wide range of ecosystem-based approaches to address societal challenges, aiming to maintain and enhance human health, quality of life, and the preservation and restoration of biodiversity (Cohen-Shacham et al., 2016). In addressing coastal flood protection, coastal wetlands and mangrove forests are a viable option. Coastal wetlands (e.g. saltmarshes) and mangrove forests can protect the hinterland by dampening the incoming waves (Jadhav et al., 2013, Möller et al., 2014, Losada et al., 2016, van Veelen et al., 2021) and adapt to SLR by capturing sediments (Ifuku and Hayashi, 1998). The reduction of wave energy due to vegetation can significantly reduce the impact on coastal structures (Vuik et al., 2016).

A Living Dike is an example of a combination of a hard structure and saltmarsh, to

enhance the flood resilience and ecosystem benefits (de Vriend et al., 2014). A Living Dike can be a remedy as a climate adaptation strategy to reinforce dike sections that do not pass the current inspection requirements and the adaptive soft solution is potentially much cheaper (Marijnissen et al., 2020). A Living Dike can dampen waves, be a habitat for ecology, sequestrate carbon, can grow with sea level rise and provide a place for recreation (Barbier et al., 2011). For a schematic representation of a dike fronted with a saltmarsh, see Figure 1.2.

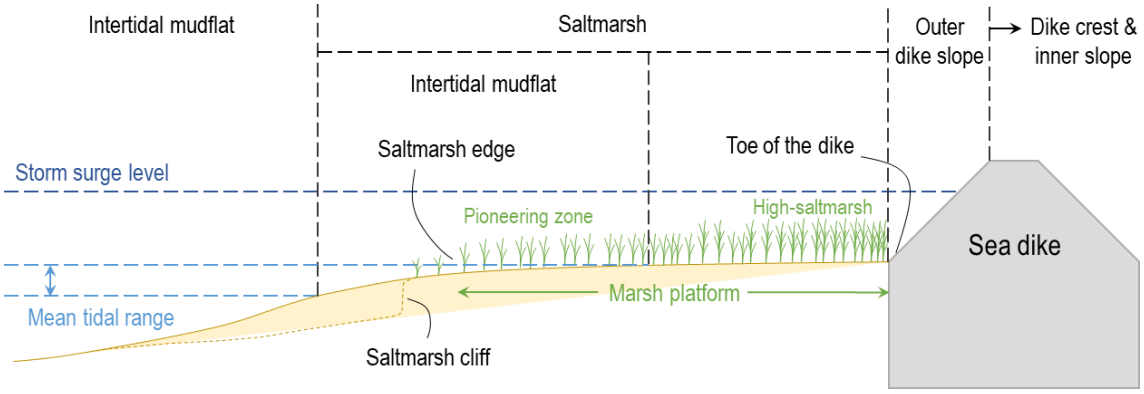

FIGURE 1.2: Schematic drawing of a dike fronted with a saltmarsh (Muller, 2022)

1.2 Problem definition

Erosion at the outer toe of a dike is crucial to understand. It represents a weak point where the stability of the dike can be compromised, potentially leading to dike breaches. The toe can be built from clay to function as a seal to prevent water from infiltrating into the dike (Piontkowitz and Chistensen, 2012). The added weight and increased water pressure from infiltration can trigger different failure mechanisms, like shear failure, especially if the water level decreases rapidly after infiltration, reducing the counter-pressure that supports the dike (Zwanenburg et al., 2011). The risk of piping (internal erosion), and slope instability also increases when a scour hole is present (Mai et al., 2006). Erosion occurs when the soil's critical shear velocity (u_{crit}) is consistently surpassed, which can lead to the development of a scour hole (Hoffmans and Verheij, 1997).

Several studies have quantified the orbital velocity at the bed and near a sloped coastal structure (e.g. Airy (1841), Van Gent and van der Werf (2014), Soulsby (2006)). However, the these approximations do not take into account the effect of a (vegetated) saltmarsh and the additional dissipation this causes. A detailed explanation of these theories is given in Chapter 2.

To writers knowledge, quantification of the near-bed orbital velocities, and the corresponding scour at the toe of a dike is lacking. Limited knowledge about quantifying the near-bed velocities and erosion of the saltmarshes and wave-structure interactions of hydraulic structures, and some approximations for the orbital velocity are present, but the exact hydrodynamic processes and interactions regarding the transition zone of a vegetated saltmarsh and a hydraulic structure are lacking. Furthermore, the effect of the slope of the structure is also unknown.

1.3 Research objective and questions

The objective of this research is to understand and quantify wave-driven near-bed flow velocities at the toe of a dike and how this varies with water levels, wave characteristics, vegetation and dike configurations. To execute the research, the following research question is formulated to achieve the research objective:

1. What are the characteristics of wave-driven near-bed velocities during storm conditions at the transition zone between a saltmarsh and coastal dike?
   (a) What is the effect of different water levels and wave characteristics?
   (b) What is the relation between the standing saltmarsh vegetation and flow velocities?
   (c) What is the effect of different dike configurations?
2. How effectively can the near-bed velocities at the transition zone between a saltmarsh and a coastal dike be captured and modeled?
   (a) How accurately can an ADV measure near-bed orbital velocities in vegetation?
   (b) How accurately can a phase-resolving non-hydrostatic numerical model simulate near-bed orbital velocities in environments with and without vegetation?

1.4 General approach

This study analyses measurements conducted in the Deltaflume at Deltares, Delft. The measurements contain near-bed velocity measurements at the toe of a dike, fronted with a saltmarsh. A data analysis is conducted on these measurements for various storm conditions. The obtained data from the Deltaflume, is used to calibrate a numerical SWASH model. The model is then used to extend the range of the tested hydrodynamic conditions within the dataset. These simulations are used to obtain insights in near-bed velocity behavior for different dike slopes and different $\frac{H_{m0}}{h_k}$ values.

1.5 Reading guide

This MSc thesis focuses on understanding the wave-driven near-bed orbital velocities at the toe of a dike. Chapter 2 gives some more background information about the current state of the art of near-bed orbital velocities, used theoretical methods and gives some useful background information. Chapter 3 will explain the methods used in this study for the analysis of the measurements carried out in the Deltaflume and for the setup and application of the numerical model with and without vegetation. Chapter 4 contains the results of Deltaflume measurements and figures concerning the velocities, and Chapter 5 contains the results of the numerical modeling and extra analyses concerning $\frac{H_{m0}}{h_k}$ ratios. The results are discussed in Chapter 6, combining the lab data analysis and numerical modeling. Chapter 7 presents the conclusions by answering the research questions. Chapter 8 gives the recommendations for further research.

2 Theoretical background

2.1 Erosion of saltmarshes

Due to storm conditions, saltmarshes and the transition point of a saltmarsh and a dike slope are prone to erosion. The protection of saltmarshes is challenging since these are complex and dynamic systems, which are influenced by biological and physical factors. The processes that support the marsh development also contribute to the degradation (Townend et al., 2011). Key factors influencing the growth and decay of the marshes are setting of the soil, hydrodynamics, sediment supply, erosion, sedimentation, morphology, saltmarsh ecology and the anthropogenic impacts (Morris et al., 2002, Kirwan and Megonigal, 2013). Long-term erosion is influenced by gradual SLR, sediment supply, climate change and land use, whilst the short-term erosion is driven by waves, storms and the tides (Wang et al., 2023). Waves have a dual effect on saltmarshes. The first effect is marshes help to dissipate wave energy, providing coastal protection. And the second effect is the impact of waves potentially damaging vegetation. Understanding these effects requires knowledge of surface topography and storm patterns (Möller et al., 2014). Vegetation also influences flow patterns, enhancing sediment settling and reducing erosion (Möller et al., 2014).

After the waves are propagated over the marsh, the waves interact with the dike. This was studied as wave-structure interactions by Schüttrumpf and Oumeraci (2005). The wave-structure interaction processes are identified into 5 zones, depicted in Figure 2.1. In zone 1, waves are propagating over the seabed, interacting with the bottom boundary layer, resulting in energy dissipation due to bottom friction (Johnson and Kofoed-Hansen, 2000). Zone 2 introduces potential wave impact pressure to the structure with return flow on the toe of the dike, the magnitude of this impact is approximated by numerical models or empirical formulas. In Zone 3, wave run-up and run-down generate near-bed velocities at the toe and along the slope of the dike. Generally, steeper slopes produce higher near-bed orbital velocities at the toe of a dike, because more wave energy arrives unbroken, and reflection is stronger. Conversely, milder slopes dissipate wave energy across a larger surf zone region, leading to lower near-bed velocities at the toe (Van Der Meer et al., 1994). Erosion potentially occurs when the critical velocity of the substrate is exceeded, typically the velocities are determined using experimental measurements and by analyzing the wave behavior.

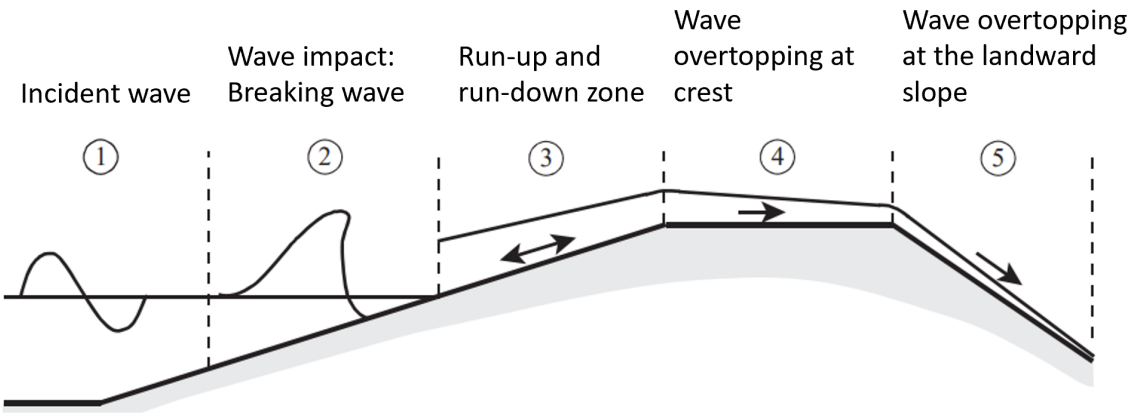

FIGURE 2.1: Wave-structure interaction processes, divided into 5 sub-flow domains (Schüttrumpf and Oumeraci, 2005)

The hydrodynamics at the toe of the dike, where incident waves, breaking waves and the run-up and run-down over the structure come together, are hard to predict due to their complex interactions. Scour at the outer toe of a dike, is defined as local scour in literature. Local scour refers to the erosion or lowering of the seabed directly around a structure, caused by the acceleration and deceleration of near-bed velocities, along with the turbulence (vortices) that results in increased local sediment transport (van Rijn, 2023).

2.2 Near-bed orbital velocity predictions

The following theories are used in this thesis to asses the accuracy of predicting the near-bed orbital velocity at the toe of a dike:

1. Linear wave theory (Airy, 1841)
2. Van Gent and van der Werf, 2014
3. Soulsby exponential approximation (Soulsby, 2006)

Each theory is described below and plotted for the known wave parameters for the tests without vegetation. The theories are only calculated with the wave characteristics of the tests without vegetation, because the vegetation introduces an extra term of dissipation which is not accounted for in these theories.

Linear wave theory

The goal of linear wave theory is to describe the motion of surface waves on a fluid, in a relatively simple way. Linear wave theory is derived by applying the governing equations of motion to an incompressible, inviscid fluid and assuming irrotational flow, allowing the velocity to be represented by a potential that satisfies Laplace's equation. By linearizing the boundary conditions for small-amplitude waves, a dispersion relation is obtained, which links wave frequency and wave number and enables calculation of wave properties Holthuijsen, 2007. By deriving a formula from linear wave theory for progressive waves as explained by Airy, 1841, a formula for the orbital velocity at the bed can be obtained. To obtain the amplitude of the orbital velocity at the bed the equation of linear wave theory can be rewritten for $z = -d$, with the formula for the amplitude parallel to the bed being:

$$\hat{u}_x(z) = \underbrace{\omega a \frac{cosh(k(z+d))}{sinh(kd)}}_{\text{Amplitude}} \underbrace{cos(\omega t - kx)}_{\text{Oscillator}} \tag{1}$$

Equation 1 can be branched into two parts, the part that decides the amplitude of the velocity, influenced by the angular frequency, wave number, wave amplitude and water depth. The oscillator describes the time dependent oscillation of the wave, oscillating between -1 and 1. This describes the cyclic behaviour of the wave over time and space. In this case ωt describes the temporal changes and kx describes the spatial phase of the wave. The rewritten equation for the velocity at the bed is:

$$\hat{u}(z = -d) = \omega a \frac{1}{sinh(kd)} cos(\omega t - kx) \tag{2}$$

To calculate the velocities relating to the JONSWAP energy spectrum that corresponds to the experiments significant wave height and period, the amplitude can be calculated using:

$$a(f) = \sqrt{2S(f)} \tag{3}$$

This equation makes sure that the amplitude of the wave is dependent on the energy that is given in the JONSWAP spectrum, and thus varies per frequency in time. Substituting Equation 3 and the angular frequency ($\omega = 2\pi f$), an equation for the orbital velocity at the bed without the oscillator is:

$$\sqrt{2S(f)\left(\frac{2\pi f}{sinh(\frac{2\pi d}{L})}\right)^2} \tag{4}$$

To obtain the velocities corresponding to the JONSWAP spectrum, the oscillator term is reintroduced, varying in time only because the velocity is observed at a certain location (depth), approximating a random sea state. This means kx is omitted, and for the ωt term the the random phase/amplitude model described in Holthuijsen, 2007 is added. This means random phases are added to the oscillator term in time. Resulting in:

$$\hat{u}_{bf} = \Sigma_{i=1}^{N}\sqrt{2S(f)\left(\frac{2\pi f}{sinh(\frac{2\pi d}{L})}\right)^2} cos(2\pi f t + \alpha_i) \tag{5}$$

Where α_i are random phases uniformly distributed between 0 and 2π. However, if the experiment is to be repeated with the random-phase/amplitude model with identical conditions, the time record would be different, just as the amplitude spectrum. In order to remove this sample character, the simulation should be repeated many times, and take the average of the results (Holthuijsen, 2007). A Monte Carlo simulation is conducted for each set of wave conditions with a 1000 simulations. Simulating 1000 random waves results in the following prediction of the highest 2% orbital velocities at the bottom ($u_{2\%}$) shown in Figure 2.2.

It should be noted that linear wave theory does not take into account the effects of bed

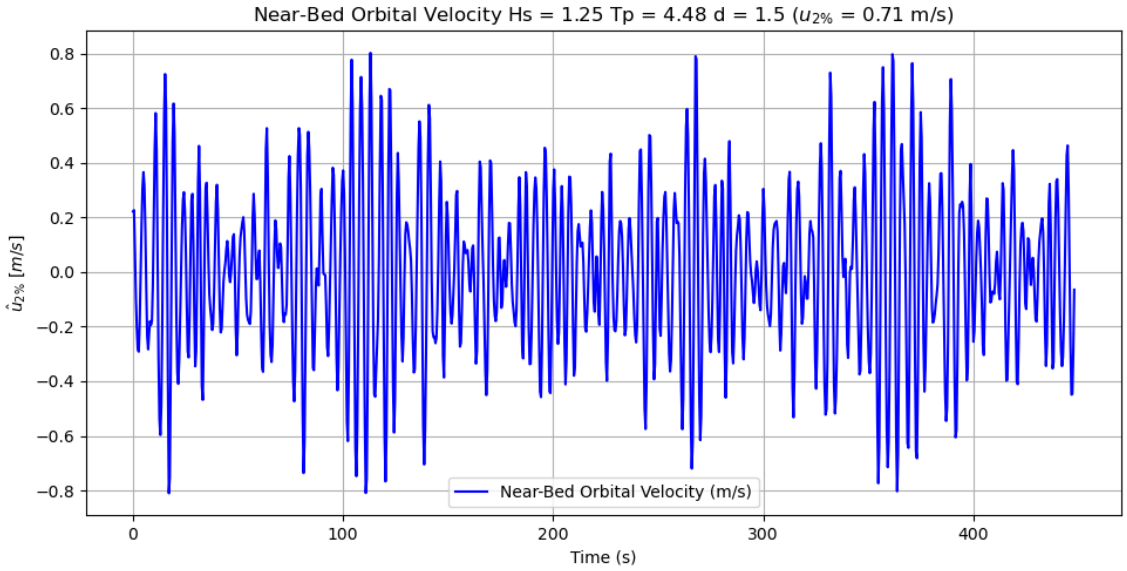

FIGURE 2.2: Example of $\hat{u}_{2\%}$ using the random phase/amplitude model

friction and it is limited to flat beds (Simarro, 2024). Linear wave theory assumes inviscid flow, i.e. it neglects the effects of viscosity and frictional forces. In reality the bed friction is an important factor in wave dynamics in shallow waters, it causes energy dissipation as the waves are propagating, creates a wave boundary layer near the seabed and it generates bed-shear stresses that can potentially cause erosion. Hence, we expect lower

velocities with the ADV-measurements due to these neglected interactions in linear wave theory.

Van Gent and van der Werf, 2014

This study examimes the velocities at the toe of a breakwater, but takes into account H_{m0} and $T_{m-1,0}$ to calculate the 2% value of the shear velocity at the toe of the breakwater. This calculated value is an input for damage assessment formulas for rubble mount breakwaters. The data is obtained from a wave flume test with a widht of 1m, height of 1.2m and a length of 110m at Deltares, Delft. The wave generator has an active reflection compensation option to prevent re-reflecting of the waves to obtain realistic wave conditions. Several different tests are conducted and widths of the toe are varied. Also different wave parameters and water depths are assessed. This study suggests that taking the non-linear effects of shallow water does not improve the estimates of the velocities at a toe structure. The following equation is proposed:

$$\hat{u}_\delta = \frac{\pi H_{m0}}{T_{m-1,0}} \frac{1}{\sinh k h_t} \text{ with } k = \frac{2\pi}{L_{m-1,0}} = \frac{2\pi}{\frac{g}{2\pi} T_{m-1,0}^2} \tag{6}$$

This estimation is based on linear wave theory for the situation where there is no variation in water depth. This equation is commonly used, e.g. in Lomonaco (1997), Wallast and Gent (2003) and Van Gent and van der Werf (2014). To verify whether these velocities are an accurate estimate they are compared with measurements conducted by Nammuni Nee Krohn, 2009. This study conducted velocity measurements near a rubble mound breakwater using ADV devices with regular waves. The calculated velocities using the wave parameters measured above the toe of the dike in the Deltaflume are compared to the 2% exceedance values of the velocity measurements (see Figure 2.3).

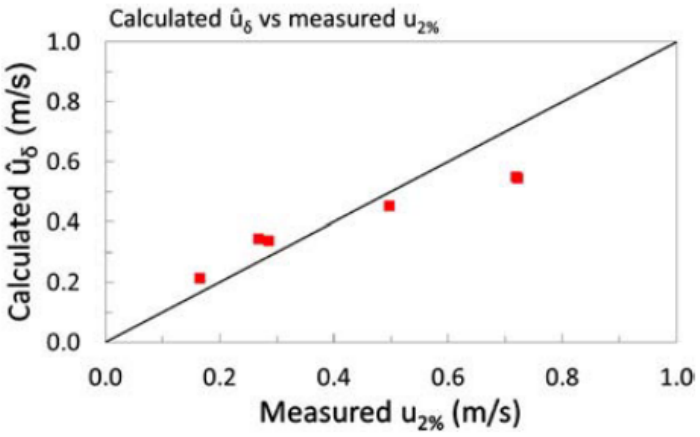

FIGURE 2.3: Van Gent and van der Werf (2014) calculation results with Nammuni Nee Krohn (2009) measurements

With the research by Nammuni Nee Krohn (2009), no significant bed shear stresses are introduced to the propagating wave. In the tests in the Deltaflume, the wave has to travel further over shallower waters, resulting in lower orbital velocities at the toe. Also return flow is not accounted for in these equations, but it is measured in the experiments. This study also only tested really small and regular wave heights and periods in comparison

to the Deltaflume experiments. Hence, this method will probably always overestimate the velocity at the toe of a saltmarsh fronted structure and this method is not suitable for this specific situation.

Soulsby exponential approximation for irregular waves

A method that incorporates the spectrum into an approximation of the amplitude of the orbital velocity is found by Soulsby, 2006. The Soulsby exponential method simplifies the estimation of near-bottom orbital velocities for irregular waves by using statistical wave parameters like significant wave height and peak wave period. It approximates the root-mean-square (RMS) orbital velocity or $u_{2\%}$ and applies an exponential decay to account for depth attenuation near the seabed. This method is useful for quick, practical estimates in environments like the velocity at the toe of a dike, without taking into account wave-structure interactions. Under natural conditions, the wave climate consists of a spectrum of waves with varying frequencies, amplitudes, and directions. Often, the only known parameters describing these sea conditions are the significant wave height (H_{m0}) and the zero-crossing period (T_z).

$$U_{rms} = \left(\frac{H_{m0}}{4}\right)\left(\frac{g}{h}\right)^{\frac{1}{2}} \exp\left(-\left[\frac{3.65}{T_z}\left(\frac{h}{g}\right)^{\frac{1}{2}}\right]^{2.1}\right) \tag{7}$$

This equation calculates the U_{rms}, by using the Rayleigh distribution we can calculate $U_{2\%}$ by using a factor $\sqrt{2} * U_{rms}$ (Soulsby, 2006).

$$u_{2\%} = \left(\frac{H_{m0}}{4}\right)\left(\frac{g}{h}\right)^{\frac{1}{2}} \exp\left(-\left[\frac{3.65}{T_z}\left(\frac{h}{g}\right)^{\frac{1}{2}}\right]^{2.1}\right)\sqrt{2} \tag{8}$$

2.3 Wave properties for irregular waves

The wave generator can either produces regular or irregular waves. A regular wave is characterized by a uniform and consistent shape and size, typically occurring in a periodic manner. An irregular wave is lacking a consistent shape, size, and timing. These waves are chaotic and do not follow a predictable pattern. In a real life situation the sea state is always irregular and unpredictable (stochastic). These irregular waves can be described as a spectrum to represent all possible observations, the spectrum refers to a range of different frequencies and amplitudes that are present in a wave field or sea state (Holthuijsen, 2007). Examples of frequently used wave spectra are the JONSWAP- or Pierson-Moskowitz spectrum.The Pierson-Moskowitz spectrum is applicable to fully developed seas, while the JONSWAP spectrum accounts for the effects of wind and wave growth in developing sea states. The latter is used for the tests at Deltares, the JONSWAP spectrum tends to offer a more realistic representation of wave conditions than the Pierson-Moskowitz spectrum, which is ideal for open ocean conditions but often oversimplifies the wave growth processes (Holthuijsen, 2007). The JONSWAP spectrum described in Holthuijsen, 2007 is defined as follows:

$$S(f) = \frac{\alpha g^2}{(2\pi)^5} f^{-}5exp\left(-\frac{5}{4}\left(\frac{f_p}{f}\right)^4\right)\gamma^r \tag{9}$$

Where $S(f)$ is the spectral energy density [m^2/s], α is a coefficient related to the significant wave height, g is the acceleration due to gravity, f is the frequency of the wave, f_p is the

peak frequency, γ is the peak enhancement factor (generally 3.3), r is a dimensionless parameter that varies with frequency:

$$r = exp\left(-\frac{(f - f_p)^2}{2\sigma^2 f_p^2}\right) \tag{10}$$

Where σ is the spectral width parameter, which takes values of 0.07 for $f \leq f_p$ and 0.09 for $f > f_p$. With these equations the JONSWAP spectrum for each of the tests can be calculated using H_{m0}, T_p and L_0. The α coefficient can be calculated using the significant wave height:

$$\alpha = \frac{H_{m0}^2}{16gT_p^4} \tag{11}$$

And the peak frequency (f_p) is calculated using the spectral peak period (T_p):

$$f_p = \frac{1}{T_p} \tag{12}$$

These equations can be used to calculate the corresponding JONSWAP spectras for each of the conducted tests, and used to calculate the orbital velocities using linear wave theory at the toe of the dike. The JONSWAP spectra used for all the conducted tests are shown in Figure 3.5. The significant wave height has the greatest contribution to the maximum spectral density where the peak period mainly determines the frequency distribution.

2.4 Measurement principle of Acoustic Doppler Velocimetry (ADV)

An ADV is a device used to measure the velocity of water or other fluids. It works by emitting sound pulses and analyzing the frequency shifts (Doppler effect) of the reflected sound waves from particles in the fluid in a certain cylindrical volume. A visualization of the measured frequency shift is shown in Figure 2.4. The ADV calculates the velocity of the fluid based on the changes in frequency, providing three-dimensional velocity measurements (u, v, w). The particles required to generate reflections of the acoustic signal can include naturally occurring suspended sediments, such as those found in rivers, oceans, or sand filled or polluted model basins. They can also be bubbles introduced by pump systems, which is often the case in flumes, or artificially added particles, known as "seeding" (Nortek AS, 2018). In the case of these experiments, the installed saltmarsh blocks provided enough suspended sediment and vegetation for the ADV to function properly.

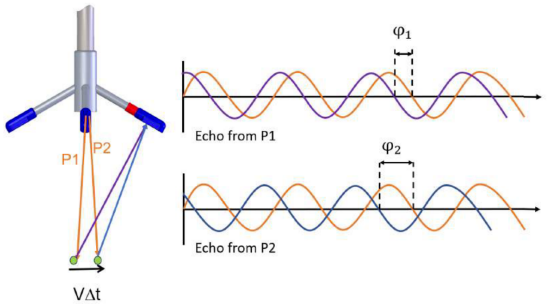

FIGURE 2.4: Phase difference visualization (Nortek AS, 2018)

2.5 Velocity profiles in varying water depths

An important understanding for this study is how the velocity profile changes for varying water depths and corresponding water conditions. As depicted in Figure 2.5, the orbital velocity path is different for varying conditions. In shallow waters the horizontal magnitude is dominant, where in deep waters the horizontal and vertical magnitudes are equal. The change in dominant magnitude is caused due to the introduction of the bottom friction. The condition is determined by the following:

$$L = \frac{gT^2}{2\pi}, \quad \text{Wave Regime} = \begin{cases} \text{Deep Water} & \text{if } h > \frac{L}{2}, \\ \text{Intermediate Water} & \text{if } \frac{L}{20} \leq h \leq \frac{L}{2}, \\ \text{Shallow Water} & \text{if } h < \frac{L}{20}. \end{cases} \tag{13}$$

This shows that the wave regime is an important aspect in understanding the hydrodynamics at the toe of a dike. All the conducted tests are in intermediate water-depths, requiring more detail for near-bed velocity calculations.

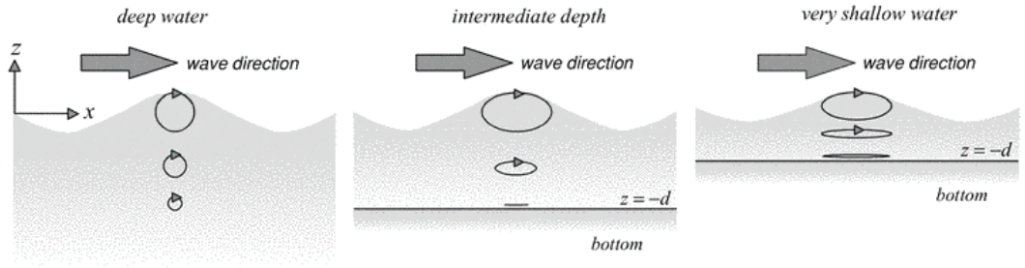

FIGURE 2.5: The orbital motion in deep water, intermediate-depth water and very shallow water (Holthuijsen, 2007)

Translating this figure into a velocity profile results into the profile shown in Figure 2.6. These profiles are also what is expected for the conducting experiments, altered by vegetation in further analyses.

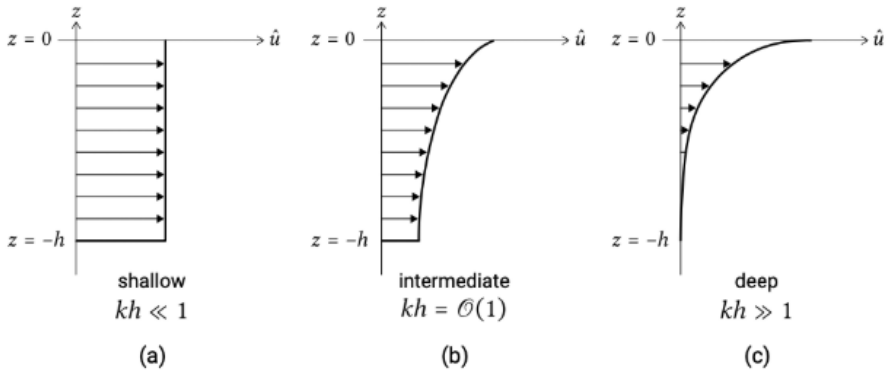

FIGURE 2.6: Schematic drawing of vertical profiles of the velocity amplitude $\hat{u}$ (Bosboom and Stive, 2023)

2.6 Welch (1967) method to determine H_{m0} and T_p

The Welch method estimates the power spectral density (PSD) by dividing a signal (wave height in this case) into overlapping segments, applying a window to each segment, and

computing the periodogram for each segment. These periodograms are then averaged, providing a smoother and more reliable PSD estimate by reducing noise and variance. An output of the this method are the frequencies of the PSD. Using the peak frequency determines the T_p:

$$T_p = 1/\text{peak frequency} \tag{14}$$

Plotting the frequencies on the x-axis and the corresponding PSD on the y-axis results in spectral density plot as shown in Figure 2.7. The zeroth moment of the spectrum (m_0) represents the total energy under the PSD curve. This is obtained by integrating:

$$m_0 = \int_0^\infty S(f)\text{df} \tag{15}$$

An important aspect of the integral to determine m_0th moment is the cutoff frequency that is adapted in the spectral plots. The cutoff frequency is important because of the presence of infra-gravity waves in the spectrum. Infra-gravity waves are an important aspect in the wave dynamics, but H_{m0} is based on wind-generated waves. The cutoff frequency used in this analysis is 0.05 Hz to eliminate the infra-gravity waves and 0.8 Hz for the upper boundary. The validation is conducted by producing results that can expand the dataset of the Deltaflume, if these results are realistic. Using m_0 the significant wave height can be calculated using:

$$H_{m0} = 4 * \sqrt{m_0} \tag{16}$$

This results in figures like Figure 2.7 for the analysis. The governing parameter that is altered determining the wave transformations in the SWASH model is the bottom friction. In this figure the change in spectral period and energy density can be observed (see Figure 2.7). The energy is the greatest at the toe, attenuating over the marsh. This is measured again at the toe of the dike, where a reduction in energy can be observed. As explained before the area of the energy density spectrum relates to the significant wave height.

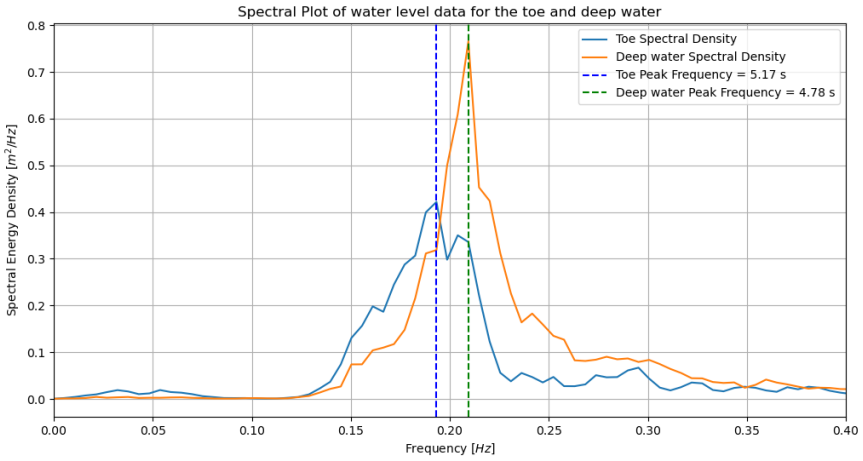

FIGURE 2.7: Spectral density from a SWASH numerical model run (deep water and at the toe)

3 Methodology

The outline of the methodology is shown in Figure 3.1. This study started with a literature study to get an understanding about how near-bed orbital velocities. Next, the velocity data measured during the Deltaflume experiments are post-processed after which each experiment was further analyzed. Using the analyzed data from the Deltaflume, a numerical model is calibrated. This calibrated model is then used to extend the measured dataset to a larger range of hydrodynamic conditions. Finally, a discussion on the results is held and conclusions on the research questions are drawn.

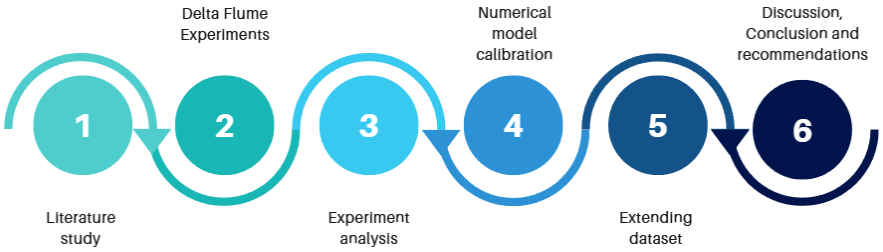

FIGURE 3.1: Methodological framework for near-bed orbital velocities at the toe of a Living Dike: Insights from Deltaflume Experiments and SWASH Model calibration

3.1 Deltaflume experiments

3.1.1 Experiment set-up

A series of full-scale wave flume tests were performed at the Deltaflume at Deltares, the Netherlands. A non-erodible dike with a slope of 1:3.6, fronted with a 70 m saltmarsh (See Figure 3.2) was placed in the flume. The saltmarsh was transplanted from a field site at the Wadden Sea coast in Northern Friesland, the Netherlands. The saltmarsh blocks were transplanted in winter state to represent the most realistic conditions of the field. To maintain the natural plant morphology and mechanical properties, salt is applied as needed to simulate a realistic environment. The vegetation is placed in two separate transects, with each transect containing a different substrate composition. This is the case because the different blocks were obtained at different locations on the marsh (i.e. one set of blocks was taken more seaward, the other set was taken more landward).

Experiments with and without vegetation at the marsh were conducted. Waves were depth-limited, simulating several sea states, ranging from 4.40m to 6.90m water depth to test low, average and extreme conditions. For the storm condition the highest possible waves are simulated (significant wave height (H_{m0}) = 2.0m), due to the waves being depth limited by the maximum possible water depth in the Deltaflume. For all simulations the JONSWAP energy distribution spectra are applied.

3.1.2 ADV set-up

Velocities at the toe of the dike (X=174.67, Z=0) were measured by an Acoustic Doppler Velocimeter (ADV). The wave height is measured offshore, near the wave paddle and near the toe of the dike using wave gauges. The attenuated H_{m0} and T_p are obtained by wave up-cross analysis of the of the wave gauges time series.

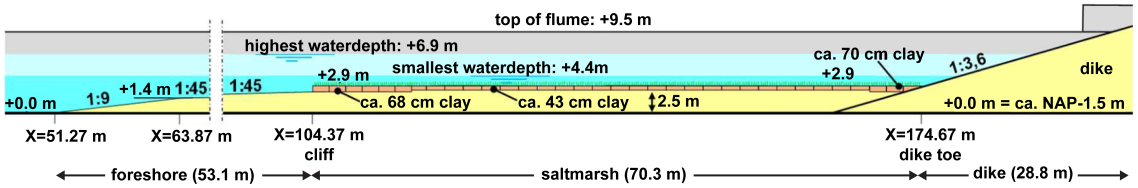

FIGURE 3.2: Experiment setup Deltaflume at Deltares (Klein Breteler et al., 2024)

The ADV (NORTEK Vector, serial number: VEC17742), is positioned in a horizontal orientation to measures the x- and y- velocities to analyze the cross shore wave-driven velocities. As this study only concerns the cross shore dynamics of the waves, the z- direction is not of interest, as it represents the width of the flume. The device is oriented with a 30 degree tilt, to mount the instrument as close to the bed as possible (see Figure 3.3). To obtain the proper velocities in the x-direction, the x and y component are combined using vector composition to obtain the velocity component u. The ADV is a high-precision device capable of measuring 3D water flow velocities in laboratory and field settings, with a measurement accuracy of approximately 1% (Nortek, 2024). It operates using acoustic Doppler technology, which sends sound pulses into the water and measures the frequency shift caused by particles moving with the water flow. The ADV device measures pulses in 3 directions at a frequency of 64 Hz. The BEAMS measure velocities in echo pulses, based on the difference in phase of the measurements, the velocity is calculated (Nortek AS, 2018). As seen in Figure 3.3, the ADV is rotated 90 degrees. This correlates to Figure 3.4, if this figure is rotated 60 degrees, the z-axis of the flume would be represented by the ADV's X with a rotation of 30 degrees axis and the x-axis plus the y axis with a rotation of 60 degrees. The measured velocities are composed into a single velocity in the x-axis direction of the flume.

FIGURE 3.3: ADV positioning (Klein Breteler et al., 2024)

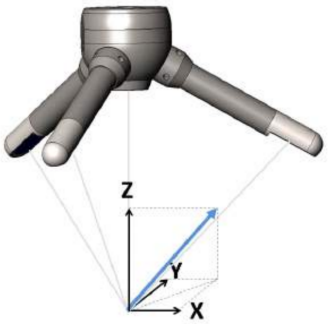

FIGURE 3.4: BEAM to cartesian (Nortek AS, 2018)

3.1.3 Test program

A series of 39 experiments have been conducted, with different wave properties following a JONSWAP spectrum. The table with all the wave properties is added in Appendix A. Variations are made in water depth (h), significant wave height (H_{m0}) and spectral peak period (T_p) determined by varying the wave steepness (s_{op}) and wave height, resulting in different hydrodynamic responses in the Deltaflume. Tests with vegetation present are conducted, afterwards the vegetation is removed by mowing and wave scenarios were

repeated. In order to obtain a reliable and robust dataset, the experiments with a 1000 waves or more are used in the analysis as in Table 3.1. The tests with different vegetation present in the flume but with the same wave properties are compared to each other to get a better understanding of the hydrodynamic responses of the waves with the given conditions. For the different wave properties, the corresponding JONSWAP spectra are plotted for each test, based on the offshore wave properties (see Figure 3.5).

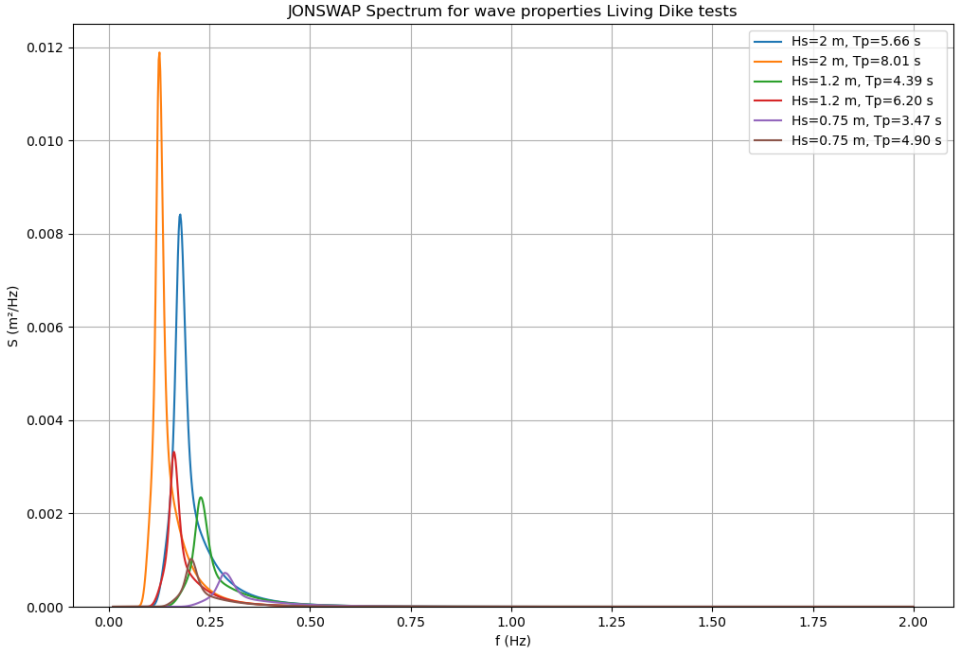

FIGURE 3.5: JONSWAP spectra of the conducted tests using H_{m0} and T_p

TABLE 3.1: Overview of experiments with corresponding offshore wave properties. *No veg* refers to the tests without vegetation present in the test flume, *Much veg* refers to the tests with vegetation present with little to no damage to the vegetation and *Little veg* refers to tests with damaged vegetation present in the test flume.

Experiment type			**Water depth**		**Offshore wave conditions**			
No veg	*Much veg*	*Little veg*	$h\ [m]$	$h_k\ [m]$	$H_{m0}\ [m]$	$T_p\ [s]$	$s_{op}\ [-]$	$L_g\ [m]$
SM-30	SM-13	SM-27	6.90	4.00	2.00	5.66	0.040	32
SM-31	SM-14	SM-28	6.90	4.00	2.00	8.01	0.020	48
SM-32	SM-09	SM-24	5.40	2.50	1.20	4.39	0.040	20
SM-33	SM-11	SM-25	5.40	2.50	1.20	6.20	0.020	29
SM-36	SM-07	SM-22	4.40	1.50	0.75	3.47	0.040	12
SM-37	SM-06	SM-21	4.40	1.50	0.75	4.90	0.020	18

All the tests are conducted with a $\frac{H_{m0}}{h_k}$ ratio of ca. 0.5. The steepness, wave height, water depth and the $\frac{H_{m0}}{h_k}$ ratio are determined in order to create realistic conditions in the Deltaflume and to research specific research goals, the varying parameters are:

1. **Water depth (h and h_k):** Varying water above the saltmarsh are tested to test the

effect of near-bed velocity dampening in different storm conditions, this helps to measure the dampening effect of the vegetation in different scenarios.

2. **Wave heights (H_{m0})**: Wave heights from 0.75 m to 2.0 m in order to simulate a broad range of storm conditions, from low storm conditions to high storm conditions respectively. This helps to quantify the effect of the wave heights on the near-bed velocities.
3. **Spectral period (T_p):** The spectral period determines the energy distribution of the waves, longer waves (higher T_p) have a different impact than shorter waves (lower T_p). Shorter waves cause more immediate damage to vegetation, while longer waves cause long-term stress. T_p influences wave height reduction, because shorter waves are more effectively damped by vegetation (Möller et al., 2014).
4. **Wave steepness (s_{op}):** Low (s_{op} = 0.02 (-)) and high (s_{op} = 0.04 (-)) slopes represent longer and shorter waves respectively. This allows to analyze the impact of different types of waves on vegetation and wave height reduction.
5. $\frac{H_{m0}}{h_k}$ **ratio:** At ratios of ca. 0.5 significant vegetation damage begins to occur, while lower ratios cause less damage (Möller et al., 2014). At higher ratios ($\frac{H_{m0}}{h_k} \approx 0.5$) the energy transfer from the waves to the vegetation is greater, leading to more damage. This is because the waves travel in intermediate waters and therefore interact more with the vegetation.

These parameters are chosen to obtain an insight in how vegetation and saltmarshes function as natural wave attenuators ans how effectively the near-bed velocities evolve for varying wave conditions and vegetation conditions. In Figure 3.6a the conditions without vegetation is shown, the vegetation is mowed down as far as possible. In Figure 3.6b, the fully grown vegetation situation is shown, and in Figure 3.6c the situation of the damaged vegetation after storm conditions is shown.

(A) *No veg* (B) *Much veg* (C) *Little veg*

FIGURE 3.6: Overview of different vegetation scenarios (*Elymus Athericus*)

3.2 ADV Data processing

The analysis focuses on understanding the wave-driven near-bed velocities at the toe of the dike under various water levels and wave conditions. The effect of wave characteristics and waterdepth will be assessed first, after which the effect of vegetation will be treated. The velocities will be plotted versus the wave power for each test (determined using local wave properties above the toe of the dike), showing the increase or decrease in wave-induced velocities to the wave characteristics for each water depth. For the tests with vegetation present, the same analysis is conducted. Resulting in plots showing the relationship between wave-induced velocities to the wave characteristics. And plots showing the change in velocities at the toe of the dike with different vegetation densities.

3.2.1 Data preparation

In order to obtain usable data from the ADV-measurement device, the data is processed using several steps, the workflow is visualized in Figure 3.7. The initial step concerns measuring the velocities using the ADV, this is conducted in the Deltaflume, at Deltares. The ADV device measures the velocities in pulse echoes in BEAM coordinates (illustration in Figure 3.4, i.e. the RAW data). The initial measurements performed by the ADV are presented in BEAM coordinates (see Figure 3.4), in order to analyse the orbital velocities, these coordinates have to be converted to the Cartesian coordinate system (X-, Y- & Z-coordinates). This is carried out using the VECTOR (version 2.00.02) software provided by NORTEK. The converted data can be further analysed trough PYTHON software. The converted data is orientated with positive streamwise velocity U towards the dike and positive wall-normal velocity W upwards (see Figure 3.3). The spanwise velocity component V is an order smaller than the other components due to the limited width of the flume and is therefore not included in the further analysis. Next, the corresponding signal to noise ratios (SNR) and correlation values will be assessed on the quality of the data. After the assessment of the SNR and correlation values a spike detection and outlier removal algorithm is applied to remove extreme outliers out of the data. The obtained data are magnitudes in three directions (X, Y and Z), these magnitudes are composed into a directional vector (directional velocity) and into velocities (parallel to the bed).

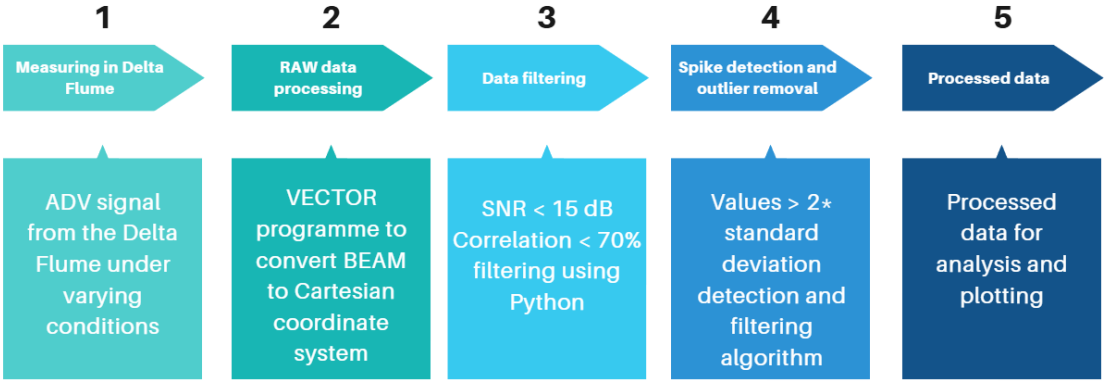

FIGURE 3.7: Process diagram ADV measurement processing

3.2.2 Signal to noise ratio

To ensure data quality and enable accurate velocity calculations, the received echo by the ADV (reflected by particles) must exceed a certain threshold. Signal strength, or amplitude, indicates the magnitude of the acoustic reflection from the water and depends on the type and quantity of particles present. Whenever the measured echo is not sufficient, the resulting calculations can be statistically "noisy". With the term noise, the background noise is intended, this noise is always a part of the measurement. This noise can lead to short term variability in the velocity dataset (Nortek AS, 2018). The instrument outputs the signal strength in relation to the background noise, which can be used to evaluate the quality of the data. The strength of the signal is assessed as a Signal-To-Noise Ratio (SNR) from Nortek AS, 2018, defined as:

$$SNR = 20\log_{10}\frac{\text{Amplitude}_{signal}}{\text{Amplitude}_{noise}} \tag{17}$$

A general guideline is that SNR must be >15 dB according to Nortek AS (2018) . In this experiment, a SNR > 15 dB is sufficient, meaning all values < 15 dB are removed from the dataset. The SNR distributions for tests with and without vegetation differ significantly. In tests with vegetation, more data needs to be excluded from the dataset. This is illustrated in Figure 3.10 and Figure 3.11, which compare the SNR for tests with and without vegetation. Both tests have the same wave properties: $h = 5.4m$, $H_{m0} = 1.2m$ and $T_p = 4.39s$. For the test without vegetation, no data needs to be removed due to the higher SNR observed in the measurements.

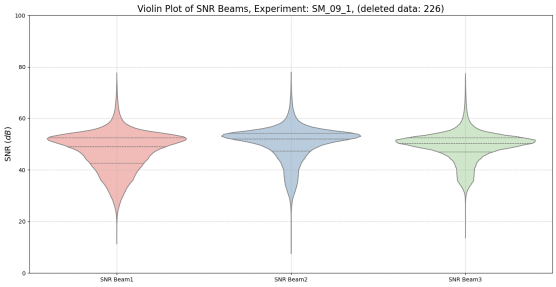

FIGURE 3.8: SNR of test SM-09-1 (with vegetation)

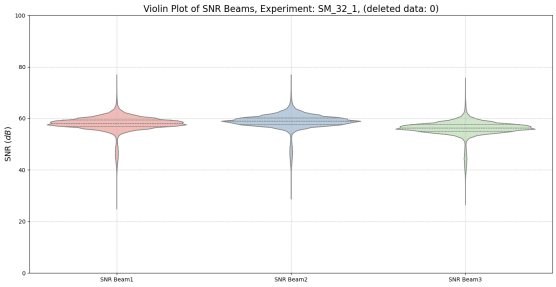

FIGURE 3.9: SNR of test SM-32-1 (without vegetation)

3.2.3 Correlation

Correlation measures how similar two consecutive pulse echoes are. A correlation of zero indicates that there is no similarity between the echoes, while a correlation of 1 means the echoes are identical. ADV instruments report a normalized correlation value, which ranges from 0% to 100%. High correlation is desirable because it confirms that the system has accurately measured the two pulses it originally emitted and is effectively determining a valid phase shift. The lower threshold for these tests is a correlation of 70% as recommended by Nortek AS (2018). All the values lower than the 70% threshold are deleted from the dataset The differences in the measured correlation values for the test with and without vegetation are shown in Figure 3.10 and Figure 3.11. The difference in correlation is significant when comparing the experiments with vegetation to the experiments without vegetation. The measurements with vegetation show less correlation than the measurements without vegetation present. This is caused by the vegetation interfering with the beam measurements, causing a local shift in some of the pulses, which results in a lower correlation value, . When submerged plants are present in the flow, additional turbulence is created and movement around the ADV's sampling volume. This movement introduces false signals, which often reduces the correlation of the velocity data and lowers the signal-to-noise ratio (SNR) by generating noise from the vegetation's constant motion. This is described in Lane et al. (1998) as low correlations tend to be associated with highly turbulent flow or large individual particles or interference which can reduce the coherence of the signal.

3.2.4 Spike detection and removal

Aside data quality checks such as Signal-to-Noise and correlation checks, the filtered data still contains outliers as a result of measurement errors. This can be caused by obstruction of the sent and/or receiving echos due to oscillating leaves of the vegetation or non-

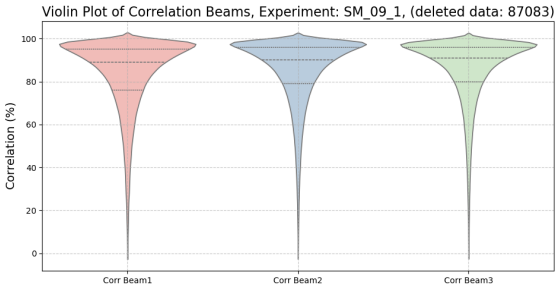

FIGURE 3.10: Correlation of test SM-09-1 (with vegetation)

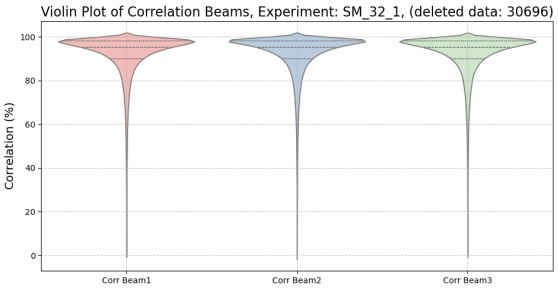

FIGURE 3.11: Correlation of test SM-32-1 (without vegetation)

physical measurement errors. In order to address the presence of outliers, a robust filtering technique is applied on the datasets. As visualized in Figure 3.12, the data contains a lot of noise and outliers. The filtering technique is particularly important in measurements subject to disturbances, like wave-induced turbulence near the floor bed or the interference of vegetation affecting the ADV. The method combines two well known concepts, i.e. the moving median and the standard deviation (std). The moving median measure is a method that is less sensitive to extreme value in comparison to the mean, this makes the moving median especially suitable for smoothing noisy data and filtering out spikes. To complement the moving median, the standard deviation of the moving median is used as a measure of variability in the data, offering a dynamic range for detecting extreme outliers or noise. A data point is classified as an outlier if a measurement falls outside the following range:

$$movingmedian(rawdata) \pm 2 * std \tag{18}$$

This algorithm ensures that points that are significantly deviating more than 2 standard deviations from the local median are flagged as an outlier. Using 2 times the standard deviation is a common threshold in statistical analysis and captures approximately 95% of the normally distributed data.

After an outlier is identified it is replaced by Non numerical number (NaN), as interpolating values introduces an extra dimension of uncertainty in the dataset.

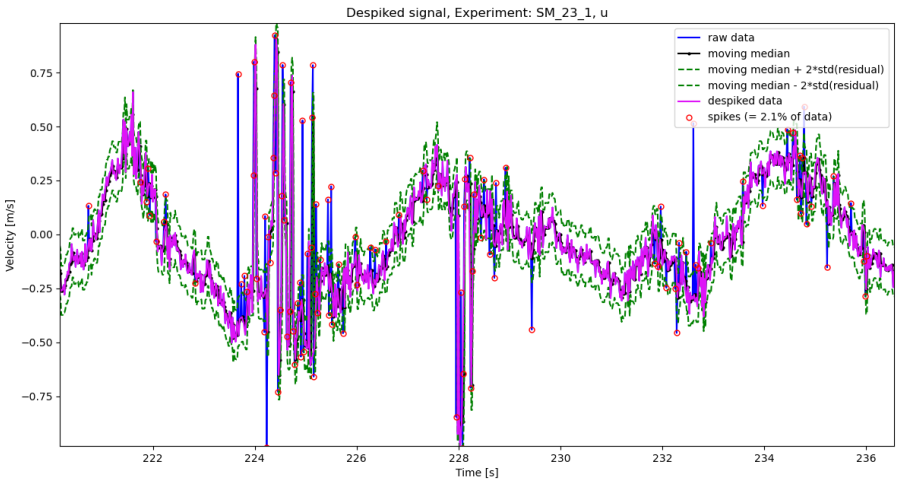

FIGURE 3.12: Experiment SM-23-1 with extreme outliers present in the data-set

After the outliers are removed, another moving median filter with a window of 64 (i.e. 1 s at sampling rate of 64 Hz) is applied to get rid of turbulent motions in the filtered dataset. This is mostly due to the scope of this thesis being the maximum orbital near-bed velocities, rather than turbulent processes. Realistically, the change of velocity is not abrupt but a smooth function in time. To solve this a Gaussian filter with a sigma of 1 can be applied on the results of the moving median filter (the combination is the Moving Gaussian Filter). This results a smooth transition of the velocity data in time in the X and Z direction (see Figure 3.13). In the used dataset, V is the velocity on the x-axis (cross-shore component) and U is the velocity on the z-axis in the height of the flume. It seems like some significant high velocities are removed by the moving median filtering, however these velocities are only present for $\frac{1}{64}$th second. Possibly this is noise by suspended particles or vegetation in the water column, obstructing the signal. These points need to be removed. The velocities parallel to the bed are the point of interest of this research, this means the V component is assessed in this case. This V component is composed from x and y directional measurements from the ADV device. Also the highest mean and wave oscillating velocities are assessed and not necessarily the turbulent velocities, hence a more smooth velocity dataset is desirable.

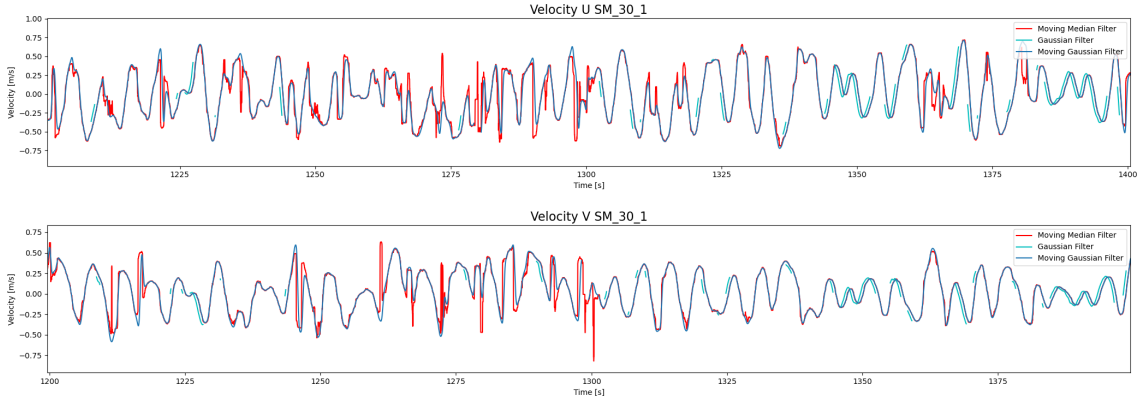

FIGURE 3.13: Processed velocity signal after moving median- and gaussian filtering of SM-30

3.2.5 Representative velocities

The wave height influences the near-bed orbital velocity, higher wave heights usually correspond to higher near-bed velocities. The relationship between wave height and near-bed orbital velocity is direct, higher wave heights result in stronger near-bed orbital velocities. This is because larger waves carry more energy, which drives increased oscillatory motion near the seabed (Bosboom and Stive, 2023). In assessments and the design of hydraulic structures, usually the significant wave height is normative. A derivation that results from the significant wave height is the orbital velocity. Hence, in this study, the significant orbital velocity is assessed as a it correlates to the significant wave height. The significant wave height refers to the mean of the largest 33% of the incoming waves passing trough a point (Hashim et al., 2016). In wave data, larger waves are more "significant" than the impact of smaller waves.

However, in this study, storm conditions and extreme events are studied. So the top 2% orbital velocities are also an important piece of interest. In other studies concerning storm conditions, the $H_{2\%}$ are assessed and sometimes describe the potential damage more

accurately (Van der Meer, 2021). In this study, only the near-bed velocities are studied. This will be called $\hat{u}_{2\%}$ for the highest 2% velocities. The 2% refers to the values that are exceeded by 2% of the waves in a certain sea state. Higher orbital velocities lead to higher shear and potential erosion. However, other equations use the H_{m0} value. In terms of the velocity component, the significant shear velocity is called $\hat{u}_{33\%}$ in this study. Both values have a point of interest due to the applications in varying equations (Van der Meer, 2021). The $\hat{u}_{2\%}$ values are shown in the main text and analysis, the $\hat{u}_{33\%}$ are added in the appendix.The Root Mean Square Error (RMSE) value is used as a quality control number (Figure 4.2), the low RMSE value corresponds to the best performing method in comparison to the measurements. This can indicate if an existing method is suitable for predicting the near-bed velocity accurately. This results in a plot showing the RMSE of each of the approximations to check accuracy in predicting near-bed orbital velocities at the toe of the dike.

3.2.6 Wave power

For all the existing theories that are tested in this study the altered wave properties H_{m0}, L_0 and $T_{m-1,0}$, measured above the toe of the dike using the zero-up-crossing method are used as input. Zero up-crossing is a method used in time series analysis of waves to identify and measure wave characteristics, such as height and period, by counting when the water surface crosses the mean level in the upward direction. The conducted tests are performed with different wave properties as shown in **??**. The main differing factor is the water depth (h), the significant wave-height (H_{m0}) and the spectral peak period (T_p). To compare the different tests with each other and to incorporate the properties into a single number, the wave power is calculated for each set of the wave properties. To calculate the wave power (P) in [W/m], the zero up-cross analysis above the toe are used. Based on measurements of a wave gauge placed 30 m in front of the toe of the dike, the proper wave characteristics are determined using a zero up-crossing (Holthuijsen, 2007). Using this approach the wave characteristics (H_{m0}wave above the marsh) and mean wave period above the marsh (T_p) are obtained. With this data, the significant wave height above the marsh can be determined (H_{m0}) and significant period above the marsh (T_p) to calculate the actual wave power above the saltmarsh (P).

$$P = \frac{1}{16}\rho g^{1.5} H_{m0}^2 h_k^{0.5} \tag{19}$$

Using this equation the wave steepness and length are indirectly taken into account, as $H = s * L$. A general observation is that wave energy increases with greater wave height and longer wave periods in deep water. However, in the tests with high water levels, wave breaking occurs before waves reach the dike slope/toe, resulting in a lower wave power for the corresponding waves, and potentially in lower velocities. Due to incorporation of h_k, the wave power is not only determined by the significant wave height, but also due to the water level (deep- ,intermediate- or shallow waters).

3.3 Numerical model

As the measurements are limited to a $\frac{H_{m0}}{h_k}$ of ca. 0.5 and a dike slope of 1:3.6, the aim of using this numerical model is to extend the dataset of the Deltaflume measurements and to accurately predict the orbital velocities at the toe of the dike. The velocities obtained in the Deltaflume are used to calibrate the numerical model.

3.3.1 Model set-up

The numerical model that was used is the SWASH (Simulating WAves till Shore) model developed by Zijlema et al. (2011). This model is a general purpose numerical model for simulating unsteady, non-hydrostatic free-surface rotational flow in coastal waters. It is intended to predict the transformations in dispersive surface waves from offshore to the beach or hydraulic structures. SWASH uses layer depth-averaged, non-hydrostatic, free-surface Navier-Stokes equations to simulate the wave dynamics.

The non-hydrostatic mode of SWASH is used, in order to model dispersive behavior of the simulated waves better. This mode can simulate wave generation, propagation, shoaling and breaking phenomena better than the hydrostatic mode, where vertical accelerations are neglected. Also wave-wave interactions that are present due to reflection of the hydraulic structure are represented better. The incorporation of multiple vertical layers makes the 1-D model a 2-D vertical model. A dx and dz discretization is used, where dz is determined by the amount of vertical layers in the model. The option to implement multiple layers in the model makes sure to approximate vertical gradients and capture the non-hydrostatic effects more accurately. The default $k-\epsilon$ model is used as a turbulence closure model. This model approaches energy transfer of breaking and dissipating waves and provides a prediction of turbulent processes.

A high resolution at the bottom of the model is desired to capture the orbital velocities in the most accurate way. In order to get a high resolution within practical computation times that can be run locally, an equidistant layer distribution is applied. This way the model is able to solve the equations in a more efficient manner, without averaging the upper layers that predict wave height attenuation.

The default values of the wave breaking parameters are used, as this represents wave breaking realistically (The SWASH team, 2024). The frictional resistance of the bed is calibrated according to the conducted measurements of the Deltaflume. The bottom boundary in the model is considered as a smooth surface (Manning coefficient of 0.011 [$s/m^{1/3}$] for bare concrete (Engineering Toolbox, 2004)), and the saltmarsh is implemented as a different roughness values (calibrated). For a visual representation see Figure 3.14.

In order for the model to be robust and work properly for different scenarios, some model choices were made. A fixed value of dt is of 0.005 s is used in the modeling. Several non-default settings were used considering the higher order numerical schemes:

- Keller-box Preconditioner ILU
- Higher order QUICK numerical scheme
- Discret CORRDEP Higher order

Higher-order numerical schemes converge better because they have lower truncation errors, which means they approximate the exact solution more accurately with fewer grid points. These schemes capture gradients, dispersive effects, and wave propagation more precisely, reducing numerical dissipation and improving stability overall. The use of the Keller-box preconditioner with an incomplete lower-upper (ILU) factorization plays a role in stabilizing the numerical solver. This box scheme ensures accurate resolvent of the gradient and frequency dispersion (Stelling and Zijlema, 2003). The ILU preconditioner is particularly suited for large, sparse systems that arise from discretizing the governing equations of wave propagation. By approximating the full LU decomposition, LU decomposition factorizes a matrix into Lower and Upper triangular matrices for efficient solving of linear systems, while ILU (Incomplete LU) is an approximate version used as a preconditioner to accelerate and stabilize iterative solvers for large, sparse systems, such as those in wave propagation models using the Keller-Box scheme. (Zijlema et al., 2011). Another

key modeling decision is the adoption of a third-order upwind numerical QUICK-scheme for the advection terms. This scheme is chosen primarily for its increase in accuracy for the advection terms, which is a major factor in this research when observing the wave attenuation. The higher-order upwind scheme prevents unstable oscillations and ensures more stable solutions. The higher order scheme is also advised by Zijlema et al., 2011 to handle steep gradients, like the bathymetry of the physical model in the Deltaflume experiments in SWASH modeling.

The higher order CORRDEP discritization approach helps maintain stable and physically plausible solutions by introducing sufficient numerical diffusion to prevent unrealistic oscillations in the water depth (Zijlema et al., 2011). Extensive oscillations leading to negative water depths is one of the main reasons the model becomes unstable.

The Courant number chosen for the model runs is 0.4 and 0.8 for the lower- and upper threshold respectively. The model must satisfy the Courant-Friedrichs-Lewy (CFL) condition to verify stability. This condition is expressed as:

$$C = C_{min} < \frac{u\Delta t}{\Delta x} \leq C_{max} \tag{20}$$

This condition allows the SWASH model to automatically increase or decrease the timestep if necessary for solving the equations, with restricted upper- and lower boundaries. The timestep is halved when the maximum Courant number is exceeded, and doubled if the minimum Courant number is exceeded. The SWASH team, 2024 advises a smaller Courant number for high-waves, but does not specify what high waves are. The higher Courant number allows for more efficient computations, but is risking numerical- dispersion or diffusion. The Courant number is default by the SWASH model and alters the initial timestep to solve the equations for the different scenarios that are run (0.75m-2.00m H_{m0}). Initially a Δt of 0.05 [s] is used and a Δx of 0.1 [m]. The lower threshold for the Courant number is 0.05 and the upper threshold is 0.25.

To obtain the proper data certain model output is necessary to analyze the behavior of the waves and hydrodynamics. This is conducted using POINTS in the SWASH model. The first point is positioned at the first grid (x=1) of the model, measuring only the surface elevation to verify if the generated H_{m0} and T_p are properly modeled. Another point is positioned at the toe of the dike (x= 1740). At this point the surface elevation is also measured, just as the depth-averaged velocities at this point per layers. These measurements in the model, can be compared to the actual measurements of the Deltaflume. The height of the depth-averaged layers can be determined in a percentage of the total water depth at a random x grid point in the model domain.

3.3.2 Initial and boundary conditions

For the numerical model a few initial- and boundary conditions are present in the model. The model is set up in 1 dimensional mode with multiple vertical layers to accurately calculate the velocity in different layers and near the bed. This makes the model a 2-DV model. Some initial conditions vary per model run, and are thus represented in Table 3.2. The initial conditions exist of the still water level and the bottom bathymetry (see Figure 3.14). The minimum depth is set to 0.0005 m for each run, when this number is exceeded, the model stops running.

The wave boundary conditions is set by a JONSWAP spectrum, initialized by a peak enhancement factor, H_{m0} and T_p. Initialized cross-shore of the model domain. At the west-side of the model domain a wave generation boundary is set to act as the deep water wave generator, generating the JONSWAP spectrum.

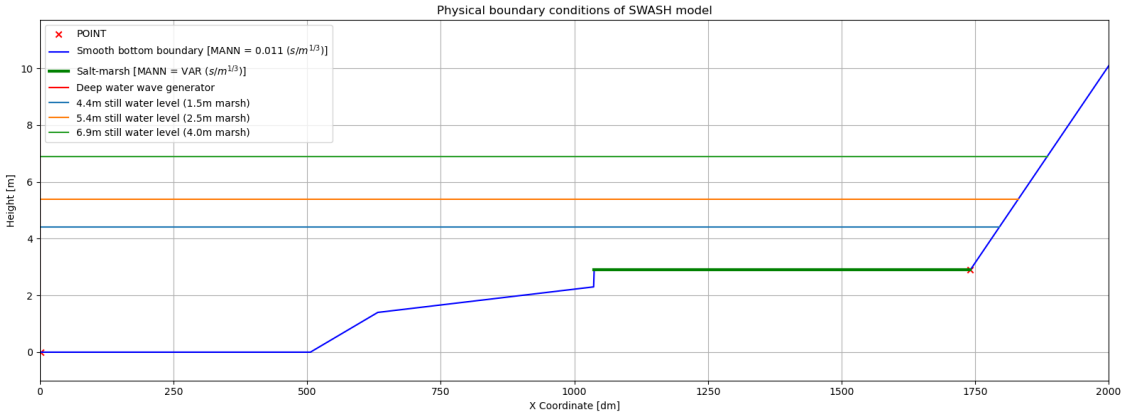

FIGURE 3.14: Bottom boundary condition in numerical model

3.3.3 Layer distribution

The model is setup as a 2-DV model using varying vertical layers. The number of vertical layers is adjusted when the water depth increases. Adjusting the number of vertical layers in 1D numerical models to account for varying water depths in the swash zone is a recognized practice. This approach enhances the model's ability to simulate complex hydrodynamic processes accurately and give a similar response in physical interactions when increasing water depth. A study by Reis et al., 2020 assessed the influence of the number of vertical layers, where the number of layers increases the models performance in reproducing H_{m0} evolution in comparison to laboratory experiments. Another study by Monteban, 2016 highlighted that increasing the number of vertical layers enhances the dispersion characteristics, broadening the applicability across various water depths. Another consideration is the accuracy of the output of the velocities, SWASH outputs depth-averaged velocities per layer. Meaning, if the layers are modeled too thick, velocities are averaged over a greater water depth. Considering the non-linear velocity profile as illustrated in Figure 3.15 & Figure 3.16, averaging too thick layers can lead to big inaccuracies.

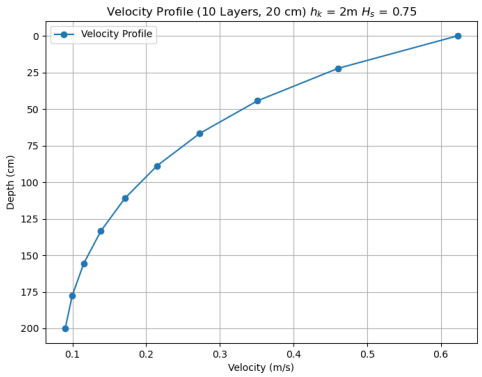

FIGURE 3.15: Low water storm conditions velocity profile

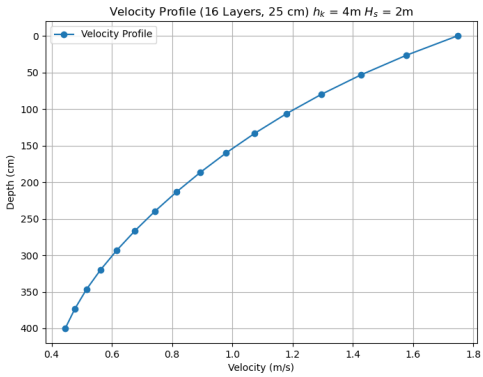

FIGURE 3.16: High water storm conditions velocity profile

The maximum amount of layers are chosen to obtain a as high as possible resolution near the bed. This results in a layer distribution as shown in Table 3.2. The layer height for every

experiment ranges between 0.20-0.21 m. This is considered as an accurate enough layer height to compare to the ADV measurements and capture the near-bed velocity accurate enough and the velocities converge. This results in 7 layers for the lowest water depths and 20 layers for the highest water depth. 20 layers is also the maximum amount of layers the model converges properly, specifically for this test case using complex bathymetry.

TABLE 3.2: Model runs, including number of layers and layer height

Layer charcateristics		**Spectral characteristics**				**Run**	**Flume**
no of layers	*layer height*	h_k	H_{m0}	T_p	S_{op}		
7	0.21	1.50	0.79	4.90	0.02	SWASH_01	SM-37
7	0.21	1.50	0.74	3.47	0.04	SWASH_02	SM-36
10	0.20	2.00	1.00	5.66	0.02	SWASH_03	-
10	0.20	2.00	1.00	4.00	0.04	SWASH_04	-
12	0.21	2.50	1.21	6.20	0.02	SWASH_05	SM-33
12	0.21	2.50	1.21	4.39	0.04	SWASH_06	SM-32
16	0.20	3.25	1.60	7.16	0.02	SWASH_07	-
16	0.20	3.25	1.60	5.06	0.04	SWASH_08	-
20	0.20	4.00	2.01	8.01	0.02	SWASH_09	SM-31
20	0.20	4.00	1.99	5.66	0.04	SWASH_10	SM30

3.3.4 Calibration and verification

In order to calibrate the model, measured offshore wave parameters of the conducted tests are the input of the model (Table 3.2). The model results should be approaching the measurements done in the Deltaflume. The wave height at the physical wave generator should be approached by the generated waves in the model, this is analyzed using the power spectral density (PSD). The PSD is determined using the Welch (1967) method. An important parameter for the model is the bottom friction, this parameter describes the shear stress at the seabed due to fluid motion. In the SWASH model, a roughness model influences the friction coefficient (C_f). The bottom friction is often used as a calibration parameter to approach measurements and calibrate the SWASH model. Roughness methods which can be applied are: Chezy formula, Manning roughness formula, Colebrook-White formula, a logarithmic wall law or a Nikuradse roughness height. Each of these methods are used in an equation to determine the friction coefficient of a model. A commonly used and standard method is the Manning coefficient. Manning uses a coefficient (n) which represents a certain type of bottom forms, the Manning roughness coefficient is advised by The SWASH team (2024) to use for oscillatory flows, as it generally provides the best representation of roughness for wave dynamics in the surf zone. When the Manning roughness is applied, the friction is determined as:

$$C_f = \frac{n^2 g}{h^{1/3}} \tag{21}$$

When calculating the bed-shear stresses using the Manning roughness formula the bed-shear stress in SWASH is computed using the formula:

$$\tau_b = \frac{1}{2} f \rho U^2, \tag{22}$$

Where the friction factor f is derived from Manning's roughness coefficient n. The relationship between f and n is given by:

$$f = \frac{gn^2}{h^{1/3}}, \tag{23}$$

Where h is the water depth and g is the gravitational acceleration. This approach accounts for bed roughness and varying water depths. The Manning's roughness coefficient (n) is an empirical parameter that depends on complex, site-specific factors such as sediment type, vegetation, and bedforms, making its selection subjective and uncertain. Furthermore, n can vary spatially and temporally due to changes in flow conditions (especially with oscillatory flows) or bathymetry, introducing additional uncertainty in numerical models (Yager, 1960)

The bare concrete is represented with a Manning roughness of 0.011 $s/m^{1/3}$ as mentioned earlier. The roughness of the bare saltmarsh is determined iteratively using different numbers of roughness. The roughness coefficient for a 'clean' earth channel is usually 0.022 $s/m^{1/3}$ (Engineering Toolbox, 2004). However, this value resulted in too much wave attenuation in the modeling. After the calibration, a Manning roughness of 0.02 $s/m^{1/3}$ is used. This value can be different from other model results due to the modeling choices made in this case. The maximum difference between measured wave reduction and modeled wave reduction is 11%.

TABLE 3.3: Model results for lowest and highest water level test with a Manning value of 0.02 $s/m^{1/3}$

Model Run	**ID**	H_{m0} **Offshore [m]**		H_{m0} **Toe [m]**	
		Model	**Flume**	**Model**	**Flume**
SWASH_01	SM-37	0.85	0.79	0.75	0.66
SWASH_02	SM-36	0.72	0.74	0.53	0.59
SWASH_09	SM-31	2.09	2.00	2.04	1.73
SWASH_10	SM-30	2.07	1.98	1.62	1.66

3.3.5 Vegetation modeling

Previously, the model was utilized without vegetation present in the model. Considering vegetation, it introduces extra wave dampening and attenuating the flow by exerting a certain drag. A visualization of the velocity profile with submerged and emerged canopy is shown in Figure 3.17. In the case of the Deltaflume tests, submerged canopy flow is present due to the drag exerted by the vegetation. A result is a significant reduction in the flow velocity inside the vegetation field, due to the interaction of the flow with the vegetation (in-canopy flow). The SWASH model allows the implementation of aquatic vegetation for wave dampening. The vegetation module needs specific input parameters to parametrize the vegetation in the model, namely:

1. Vegetation height [m]
2. Diameter of each plant [m]
3. Number of stems [$-$]
4. The drag coefficient per vertical segment [$-$]

These vegetation parameters were measured during the experiments and reported (Klein Breteler et al., 2024). However, the measurements are different from the necessary input

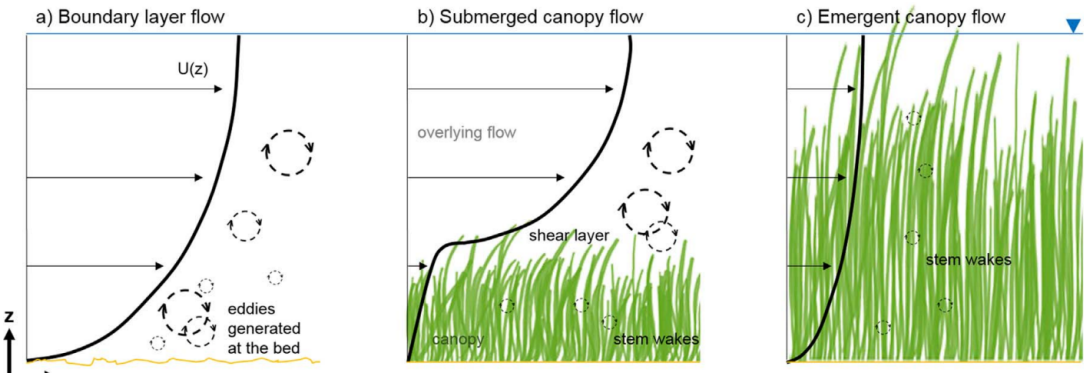

FIGURE 3.17: Sketch of three different flow regimes. The dominant source of turbulence is respectively (from left to right) the bed, the top of the canopy (shear layer), and the stem wakes (Beudin et al., 2017)

for the model. Were the number of stems, stem height and stem diameter per quadrant (20x20cm) are measured and given in the report. This is converted to the amount of kg/m^2 of dry biomass for the implementation in the SWASH model. This is converted to the number of stems per m^2, stem height and stem diameter needed as input for the numerical model. The vegetation measurements are shown in Table 3.4.

TABLE 3.4: Results of vegetation measurements from Deltaflume

Sample area [cm^2]	**Stems [no]**	**Stem length [cm]**	**Stem diameter [mm]**
20x20	33.5	17.26	18
100x100	838	17.26	18

The stem diameter measurements resulted in a diameter of 0.0018 m, agreeing with some measurements in literature (Möller et al., 2014). This diameter is used in the vegetation modeling as an input value. The vegetation is only modeled on the saltmarsh. The drag coefficient is determined as a function of the vegetation Reynolds Number (Re_v) for irregular waves, as determined by Möller et al., 2014, who also performed experiments on the same vegetation type as was present in the Deltaflume experiment (*Elymus athericus*). The equation is as follows:

$$C_D = 0.159 + \left(\frac{227.3}{Re_v}\right)^{1.615} \tag{24}$$

With:

$$Re_v = U_{max}\frac{S_D}{\nu_k} \tag{25}$$

Where S_D is the stem diameter, v_k is the kinematic viscosity for seawater ($1 * 10^{-6}\ m^2 s^{-1}$) and U_{max} is the orbital velocity at the bottom in front of the vegetated section. U_{max} is determined using linear wave theory. This means different C_d values are used for the varying water depths and wave conditions. The values of U_{max} are calculated using linear wave theory and the corresponding Re_v are calculated. From measurements the value of S_D = 1.8 mm. This results in the following values of Re_v and C_d shown in table Table 3.5 in the appendix. The variation in C_d is limited for the applied wave conditions. These vegetation characteristics are implemented in the numerical model and validated based on the measure H_{m0} and $\hat{u}_{2\%}$ in the Deltaflume. The results are wave attenuation percentages at

TABLE 3.5: Model input for vegetation modeling

Spectral characteristics				Model	Run ID	Vegetation characteristics		
h_k [m]	H_{m0} [m]	T_p [s]	$s_{op}[-]$			U_{max} $[ms^{-1}]$	Re_v [-]	C_d [-]
1.5	0.7	3.4	0.04	SWASH_V_01	SM-07	0.85	1.53E+03	0.20
2.0	1.0	4.0	0.04	SWASH_V_02	-	0.98	1.76E+03	0.20
2.5	1.2	4.4	0.04	SWASH_V_03	SM-09	1.08	1.94E+03	0.19
3.3	1.6	5.1	0.04	SWASH_V_04	-	1.25	2.25E+03	0.18
4.0	2.0	5.7	0.04	SWASH_V_05	SM-13	1.40	2.52E+03	0.18

the toe of the dike, which can be compared to the wave gauge measurements. Additionally, the near-bed velocities can be extracted from the numerical model lowest layer. The model is not calibrated, but the drag coefficient theory is tested using the existing theory by Möller et al. (2014) for vegetation modeling.

3.4 Testing different dike slopes

In order to examine the effect of different dike slopes, different slopes were tested for the lowest water level (4.4 m), intermediate water level (5.4 m) and the highest water level (6.9 m). The dike slopes that were tested are $1:3$, $1:3.6$, $1:4$, $1:6$ and $1:8$. Al slopes are tested without vegetation present in the model, to isolate the processes on the slope and ignore the dampening effect of the vegetation.

3.5 Testing different $\frac{H_{m0}}{h_k}$ ratios

The Deltaflume experiments were conducted with a $\frac{H_{m0}}{h_k}$ ratio of ca. 0.5. The calibrated numerical model without vegetation will be used to get a better understanding on the near-bed velocity component at the toe of the dike for varying ratios. The model runs that are conducted are given in Table E.1. The different scenarios are a point of interest, because the velocity profile develops differently for different ratios. Only scenarios without vegetation and s_{op} of 0.04 are considered due to lack of time. The range of wave heights is selected to obtain an as broad as possible spectrum of $\frac{H_{m0}}{h_k}$ ratios, with realistic wave height conditions.

4 ADV Measurements

4.1 Near-bed orbital velocities without vegetation

For the measurements without vegetation, the upper 2% values of the near-bed velocity ($\hat{u}_{2\%}$) are determined. and the significant shear velocity ($\hat{u}_{33}$) are assessed. The figure of $\hat{u}_{33}$ is added in Appendix F. For each experiment the amount of waves is shown in Table 4.1.The local wave characteristics at the toe of the dike are combined in the wave power and compared with the different occurring velocities(Figure 4.1).

TABLE 4.1: Offshore wave properties and number of waves for tests without vegetation

Vegetation damage	Experiment ID	H_{m0} [m]	T_p [s]	N_u [no]	Wave Power [W/m]
No veg	*SM31*	1.74	8.12	925	3.63E+04
No veg	*SM30*	1.66	5.88	1082	3.31E+04
No veg	*SM33*	1.06	6.33	1277	1.07E+04
No veg	*SM32*	1.04	4.49	1067	1.09E+04
No veg	*SM37*	0.66	5.08	1239	3.18E+03
No veg	*SM36*	0.59	3.58	1051	2.55E+03

With an increase in wave power, an increase in $\hat{u}_{2\%}$ at the toe of the dike is observed (Figure 4.1). However, this trend levels out at higher wave power experiments. This is mainly due to the increase in wave period. For the same wave heights, the same amount of mass passes over a long period, casing lower velocities. However, the wave height is still the governing parameter due to the square in the wave power equation.

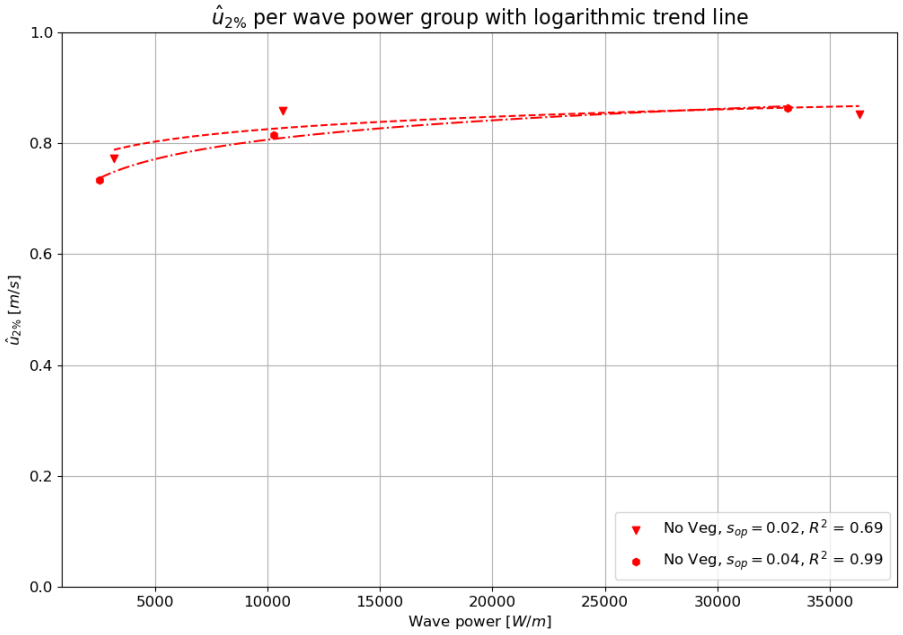

FIGURE 4.1: $\hat{u}_{2\%}$ per wave power group

The measured $\hat{u}_{2\%}$ at the toe of the dike are compared with theories or other literature for near-bed velocities in similar setups (see Figure 4.2). The theories that are tested are linear wave theory, Van Gent and van der Werf (2014) and the Soulsby (2006) exponential approximation. Linear wave theory performs the worst at predicting the $\hat{u}_{2\%}$, with an RMSE of 0.40 ms^{-1}. As described in theory, linear wave theory does not take into account the non-linear factors of wave propagation. This non-linearity is more pronounced due to the marsh and cliff being present, causing an underestimation for all the predictions. Linear wave theory is thus a bad estimator in the case of predicting near-bed orbital velocities with the presence of saltmarsh.

The Soulsby (2006) exponential approximation for irregular waves performs worse than van Gent with an RMSE of 0.24 ms^{-1} in this case. The method of irregular waves performs well in the shallow water experiments, but with greater water depths the approximation becomes less accurate. For deeper waters the approximation performs exceptionally well, but for the shallow water experiments the results are too far off to be a reliable estimator.

The method of Van Gent and van der Werf (2014) has the best performance with a RMSE of 0.18 ms^{-1} in the case of predicting the velocities at the toe of the dike. The approximation does however predict badly in the case of deep and shallow waters, but for intermediate waters it performs really well. An RMSE of 0.18 ms^{-1} is reasonable, but this implies an uncertainty of around 20 % in estimating the proper near-bed orbital velocities at the toe. This is too far off for practical use of the theories.

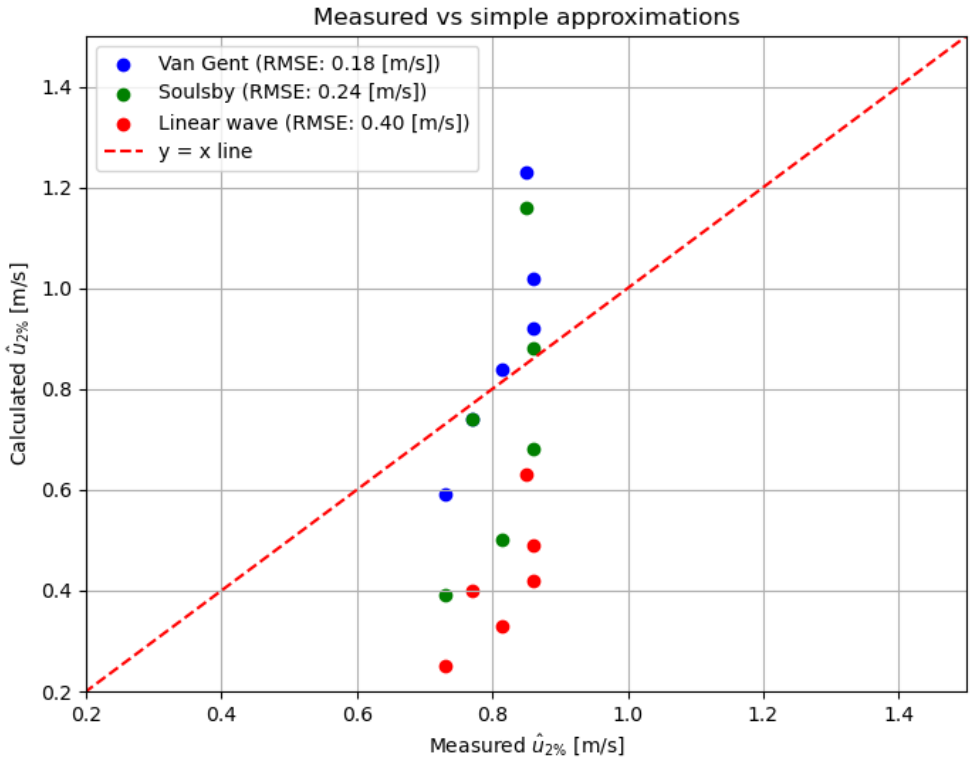

FIGURE 4.2: Overview of approximations vs measurements

4.2 Near-bed orbital velocities with vegetation

For the analysis with vegetation present in the flume, two different types of tests are conducted. One series of tests with the vegetation having no to little damage, and one series of tests where the vegetation has significant damage. Furthermore, exactly the same H_{m0}, T_p and L_0 are initiated at the wave paddle. The exact wave properties obtained by a zero-upcross analysis are shown in Table 4.2.

TABLE 4.2: Offshore wave properties and number of waves for tests with vegetation

Vegetation damage	Experiment ID	H_{m0} [m]	T_p [s]	N_u [no]	Wave Power [W/m]
Veg little damage	*SM14*	1.67	8.04	479	3.36E+04
Veg little damage	*SM13*	1.55	5.82	1012	2.9E+04
Veg little damage	*SM11*	1.01	6.34	1268	9.79E+03
Veg little damage	*SM09*	1.00	4.48	1095	9.58E03
Veg little damage	*SM06*	0.58	5.10	1860	2.44E+03
Veg little damage	*SM07*	0.48	3.60	1552	1.72E+03
Veg much damage	*SM28*	1.76	8.08	590	3.72E+04
Veg much damage	*SM27*	1.62	5.81	1076	3.17E+04
Veg much damage	*SM25*	1.02	6.33	1256	9.94E+03
Veg much damage	*SM24*	1.02	4.48	1079	9.83E+03
Veg much damage	*SM21*	0.59	5.09	1845	2.59E+04
Veg much damage	*SM22*	0.52	3.60	1586	2.00E+03

In Figure 4.3, a regression line is plotted. A logarithmic regression line has the best fit, with s_{op} = 0.02 the regression line is plotted as a dashed trend line. For s_{op} = 0.04 the regression line is plotted as a dash-dot trend line. The first observation is that the damage of the vegetation does not have a significant influence on the attenuation capacity of the vegetation (see Figure 4.3). Overall, the most significant reduction in velocity is at the highest wave power, where the vegetation has a attenuation of approximately 0.4 ms^{-1} in the x-direction. This can imply that a longer spectral period more sensitive to near-bed orbital velocity attenuation by vegetation than a shorter spectral period. Only at the lowest two wave powers, the longer period waves are attenuated more than the shorter period waves. This is probably because of the water depth, due to this depth bottom friction is more significant than the attenuation of the vegetation.

Adding to this observation is that with damage on the saltmarsh, the wave attenuation capacity of the vegetation seems relatively stable, only losing a small part of its wave-driven flow attenuation capacity (see Figure 4.3). On average, the velocities are reduced by vegetation with little damage for 52%, and due to vegetation with significant damage for about 29%. The mean difference between little damaged vegetation and significantly damaged vegetation is 23%.

4.3 Summary ADV measurements

The aim is to obtain an understanding of how water levels and wave parameters influence the near-bed orbital velocity at the toe of a dike fronted with a saltmarsh. And what the relationship between the standing saltmarsh vegetation is and the near-bed velocities.

In case of the wave heights, an observation is that higher wave heights introduce higher near-bed velocities at the toe of the dike. This is mainly due to the fact the waves are depth limited. The effect of the water depth is not explicitly obtained from the data,

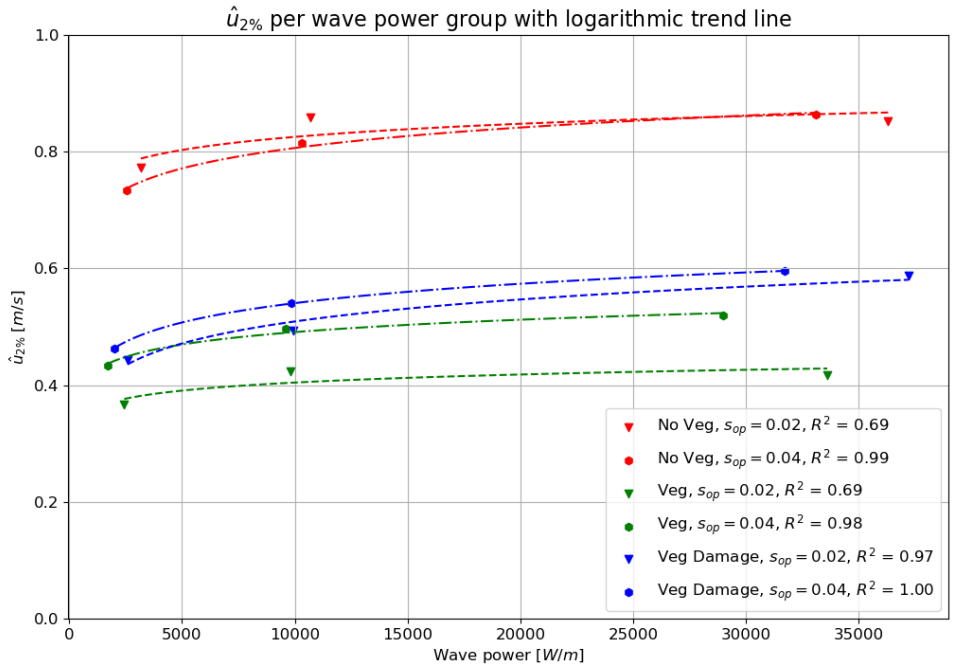

FIGURE 4.3: $\hat{u}_{2\%}$ with vegetation

because for each water level the the same H_{m0}/h_k ratio is used. This can be investigated further with a calibrated numerical model, exploring different H_{m0}/h_k ratios to gain an insight in the effect of the relationship between water depth and wave height.

Waves with a shorter wave period have a higher velocity than the waves with a longer period in the intermediate and higher water level. This is the case for the experiments with and without vegetation. This means, higher wave power does not necessarily imply higher velocities.

In terms of the relation between standing saltmarsh vegetation and the orbital velocities, a clear reduction in velocities is observed. The attenuation of the unharmed vegetation is significant (52%), with the most attenuation for the longer period waves. In terms of the damaged vegetation, the attenuation capacity reduces, but the reduction in attenuation capacity is not significant (23%). The situation in the field allows the vegetation to regrow between storm events, this affects the near-bed velocities attenuation capacity.

To estimate the velocities at the toe of the dike, the Van Gent and van der Werf, 2014 shows the best results (smallest RMSE). Acquiring these velocity estimates at the dike toe requires specific wave spectral data due to bed attenuation needs, due to the fact the attenuation of the bed needs to be incorporated. Other estimators are not really promising in predicting the results for high water levels (storm-conditions). Numerical simulations are recommended to expand the current dataset, allowing futher analysis of near-bed orbital velocities and bed shear stresses under varying wave and waterdepth conditions.

5 Numerical model

5.1 Numerical model results without vegetation

This section shows the results of the numerical model calibration, and the addition of extra data for intermediate water depths for storm conditions with an H_{m0}/h_k ratio of 0.5. The executed scenarios and the results are shown in Table 5.1.

TABLE 5.1: Results of executed scenarios SWASH modeling without vegetation

Depth	**Wave conditions**			**ID**		H_{m0} **[m]**		H_{toe} **[m]**		$\hat{u}_{2\%}$ $[ms^{-1}]$		**[%]**
h_k [m]	H_{m0} [m]	T_p [s]	s_{op} [-]	*Model*	*Flume*	*Model*	*Flume*	*Model*	*Flume*	*Model*	*Flume*	
1.5	0.79	4.90	0.02	01	SM-37	0.85	0.79	0.75	0.66	0.91	0.77	15
1.5	0.74	3.47	0.04	02	SM-36	0.72	0.74	0.53	0.59	0.74	0.73	1
2	1.00	5.66	0.02	03	-	1.06	-	1.02	-	1	-	-
2	1.00	4.00	0.04	04	-	1	-	0.76	-	0.87	-	-
2.5	1.21	6.20	0.02	05	SM-33	1.3	1.21	1.28	1.06	0.75	0.86	-14
2.5	1.21	4.39	0.04	06	SM-32	1.23	1.21	0.97	1.04	0.72	0.82	-13
3.25	1.60	7.16	0.02	07	-	1.68	-	1.6	-	0.89	-	-
3.25	1.60	5.06	0.04	08	-	1.65	-	1.29	-	0.79	-	-
4	2.01	8.01	0.02	09	SM-31	2.09	2.01	2.04	1.74	0.87	0.85	2
4	1.99	5.66	0.04	10	SM30	2.07	1.99	1.62	1.66	0.96	0.86	10

For each scenario, the spectral density spectrum is plotted (Figure G.1) to determine the spectral wave height and period using Welch (1967) method. Note that in Figure G.1i and Figure G.1j, the scale of the y-axis is different due to significant higher energy density. The spectral density plots result in a calculated H_{m0} and T_p for both offshore conditions and at the toe. With the calculated values of H_{m0}, the reduction is quantified over the saltmarsh. The relative wave reduction is also shown, in order to compare the wave height reduction of the model with the actual measurements of the Deltaflume in Table 5.1. The first H_s represents the value of the SWASH model and the second represents the H_s from experiments in the Deltaflume. The same is the case for H_t and $\hat{u}_{2\%}$.

A distinction in model accuracy can be observed for both the 0.02 and 0.04 s_{op}. For s_{op} = 0.02, the results are less accurate than for s_{op} = 0.04 . Wave attenuation waves with a steepness of 0.02 are approximated less accurate. Especially when the water depth increases, the wave attenuation capacity seems to near zero. For s_{op} = 0.02 (i.e. longer wave periods), the model is more sensitive to numerical dissipation (Zijlema et al., 2011). This model requires a finer horizontal grid to resolve the hydrodynamics more accurately, but due to time constraints this is not tested. For s_{op} = 0.04 the wave attenuation is slightly overestimated. However, the overall performance of the model is sufficient for the aim of this study.

Similar comparison is made for the calculated and measured near-bed velocities. For less steep wave (e.g. s_{op}=0.02) the model predicts the velocities less accurate compared to the measurements. The model is more accurate for s_{op} = 0.04 scenarios. For the scenarios with a s_{op} = 0.02, the deep water scenario (highest wave power) results in an accurate result for the $u_{2\%}$ value, with an inaccurate wave attenuation result. This can be due to the flow velocity profile, which is represented more accurately the layers near the bottom.

An overview is presented of the modeled and measured near-bed velocities at the toe of the dike (Figure 5.1). The wave steepness are shown with separate colors. The RMSE of the steep waves (s_{op} = 0.04) is better than the waves with a steepness of (s_{op} = 0.02). The velocities for the highest water depth matches the near-bed velocity in the Deltaflume, but the waves are not attenuated at all in the model. This makes the calculated velocities for scenarios with s_{op} = 0.02 questionable. The distinction in wave steepness is made because of the reliability of the model for the two different wave steepnesses. The velocity is obtained by analyzing the velocity measurements in the lowest layer of the model and applying the same analysis as for the velocity measurements of the Deltaflume. This results in $u_{2\%}$ value for the velocity in the lowest layer of the SWASH model.

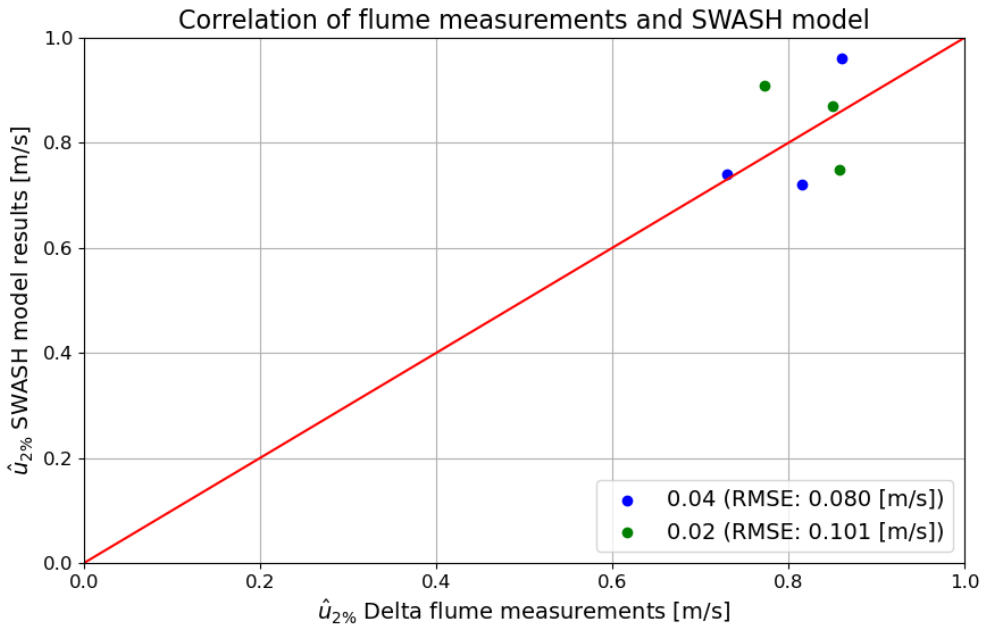

FIGURE 5.1: Correlation between ADV $\hat{u}_{2\%}$ and SWASH $\hat{u}_{2\%}$

5.2 Testing different dike slopes

For the lowest wave height, a decrease in near-bed velocity at the toe of the dike is seen as the dike slope decreases. The decreasing trend reflects the dissipation of energy on a gentler slope. For the intermediate wave heights, the velocity grows with a decreasing dike slope, but a negative trend is present towards the smallest dikes slope. Velocities increase with wave height, with a noticeable peak at a dike slope of 1:6. This suggests that moderate water levels and wave heights maximize flow energy near the toe for intermediate slopes. For the largest wave heights, the same is observed as for the intermediate trend. The relation between the near-bed velocity at the toe of the dike and the dike slope, behaves differently for different water depths and wave heights.

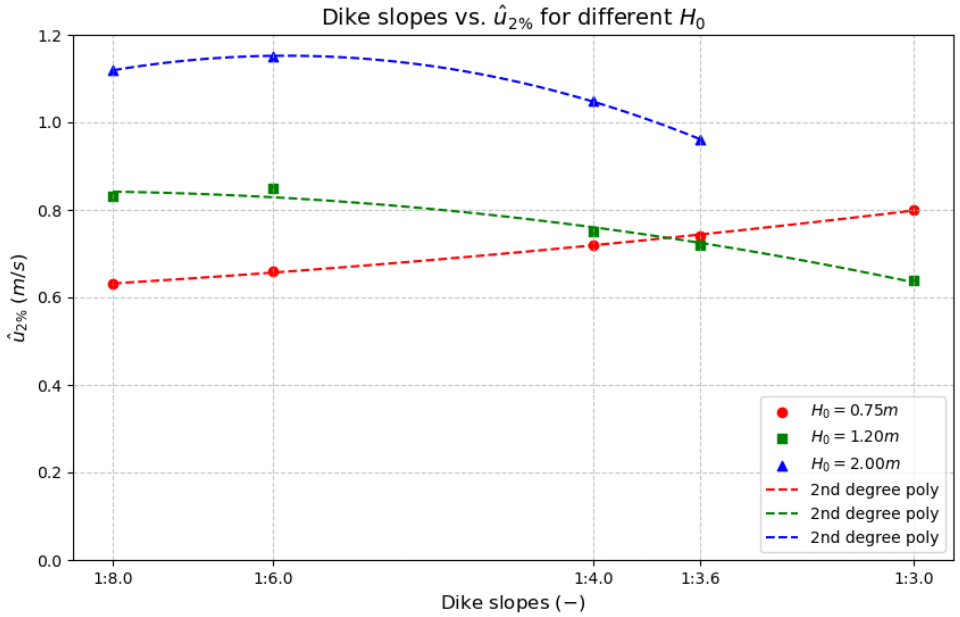

FIGURE 5.2: Evolution of $u_{2\%}$ due to varying dike slopes

5.3 Wave height - depth relation ($\frac{H_{m0}}{h}$)

For all the conducted Deltaflume experiments without vegetation, roughly the same H_{m0}/h ratio was used. However, different velocities may occur when different wave heights are propagating over varying depths. For this purpose, more wave heights are tested in the model with different H_{m0}/h values.

To obtain a further insight on the wave relation with the velocities, the model runs with different H_{m0}/h_k scenarios. Around a ratio of 0.78 wave breaking occurs in shallow water according to literature (Thornton and Guza, 1983) and the growth in velocities should be stagnating near the bed. This is tested for all the same water levels as used in the Deltaflume, but with different wave heights (Figure 5.3). A positive correlation is observed with a dependency on H_{m0}. When the wave height grows, the velocity increases until the point wave breaking is occurring, approximately at $\frac{H_{m0}}{h_k}$ = 0.8. Higher values of $\frac{H_{m0}}{h_k}$ indicate stronger wave activity relative to the water depth, causing an increased energy transfer and velocities near the bed. Larger waves carry more energy and momentum,

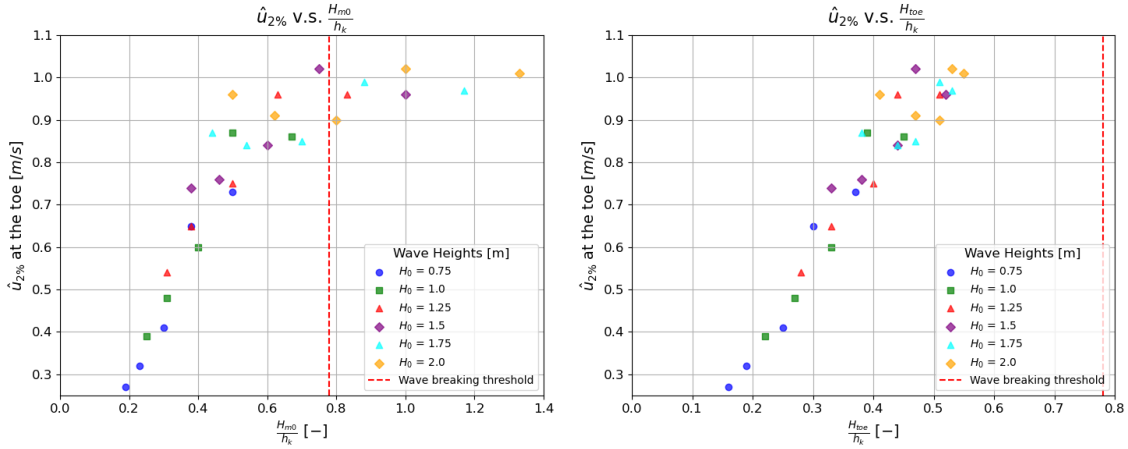

(A) Waveheight offshore (H_{m0}) (B) Waveheight above the toe (H_{toe})

FIGURE 5.3: Velocity evolution of $\frac{H_{m0}}{h_k}$ ratios for different H_{m0} measurement locations

resulting in stronger velocities. A threshold is present around the ratio of 0.8 due to wave breaking, where the wave-induced velocities do not increase any more.

The numerical model is used to extend the dataset of the Deltaflume. The model is calibrated for a certain Manning roughness value, successful for steeper waves (s_{op} = 0.04). Gentler waves (s_{op} = 0.02), with longer wavelengths are not modeled successfully, governed by numerical dispersion. Furthermore, the vegetation modeling is analyzed. This resulted in relatively low extra wave attenuation, and a bad representation of the near-bed velocity due to the depth-averaging of the per layer. The drag determination by Möller et al. (2014) does not result in realistic wave attenuation.

The different dike slopes are tested successfully and give an insight in the dynamics between water height and dike slopes in some extent. Where lower water levels near-bed velocities at the toe tend to decrease with gentler slopes, higher water levels tend to increase until a certain point. The exact dynamics of this are not clear, this can be the case due toe increased reflection, wave overtopping, increased energy dissipation for certain water depth or other wave-structure interactions like wave breaking on the slope.

The $\frac{H_{m0}}{h_k}$ tests indicate that after wave breaking at a $\frac{H_{m0}}{h_k}$ of 0.78, the near-bed velocities tend to decrease. With a maximum occurring velocity of approximately 1.0 ms^{-1}. This implies that when waves have broken, the near-bed velocity is lower at the toe.

5.4 Numerical model results with vegetation

The results of the model runs are shown in Table 5.2, and the corresponding spectral plots are shown in Figure G.2. The vegetation modeling does alter the wave height slightly, but not as significantly as should be expected. With a h_k of 1.5 m, 10% reduction is missing. The energy dissipation is decreasing when the water depth increases in the model, which should not be the case.
The corresponding spectral plots with vegetation shown in Figure G.2 look very similar to the figures without vegetation. The energy is reduced in a similar way as without vegetation present in the model, only a slight extra reduction is present in some cases.

The vertical velocity profile are shown for both shallow and deep water scenarios (Fig-

TABLE 5.2: Results of executed scenarios SWASH modeling with vegetation

Depth	**Wave conditions**			**ID**		H_{m0} **[m]**		H_{toe} **[m]**		$\hat{u}_{2\%}$ $[ms^{-1}]$		**[%]**
h_k [m]	H_{m0} [m]	T_p [s]	s_{op} [-]	*Model*	*Flume*	*Model*	*Flume*	*Model*	*Flume*	*Model*	*Flume*	
1.5	0.75	3.47	0.04	V_02	SM-07	0.72	0.75	0.53	0.48	0.67	0.43	36
2	1	4.00	0.04	V_04	-	1	-	0.76		0.8	-	-
2.5	1.2	4.39	0.04	V_06	SM-09	1.23	1.21	0.95	1.00	0.92	0.49	47
3.25	1.6	5.06	0.04	V_08	-	1.65	-	1.27		1.02		-
4	2	5.66	0.04	V_10	SM-13	2.07	2.01	1.6	1.55	1.15	0.51	56

ure 5.4 & Figure 5.5). In these plots, h_k = 0 represents the water surface on the x-axes. The velocity for V-02 looks like the theory describes, with a boundary layer developed in the lower layers. This scenario does not overestimate the velocity significantly. When the water depth increases, the averaging of the velocities per layer becomes too coarse, causing an overestimation in velocities in the lower layer (all the layers). The velocity profiles is expected to look similar to the profile depicted in Figure 3.17. The near-bed velocities are not well represented in the numerical model with vegetation and are overestimated significantly (Table 5.2). These results suggest that this is due to the depth-averaging per layer of the velocities in the model. Increasing the resolution near the bottom (through a logarithmic layer distribution) this problem could be solved. Model simulations were run with this layer distribution, but suffered stability problems.

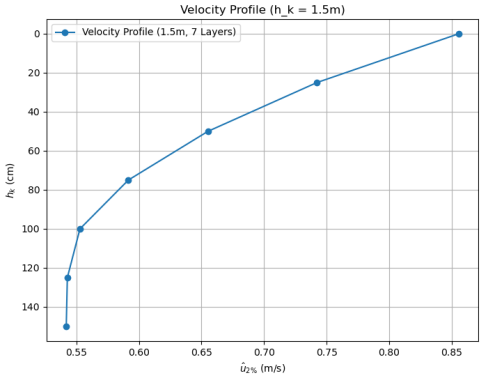

FIGURE 5.4: Velocity profile for SWASH-VEG-02

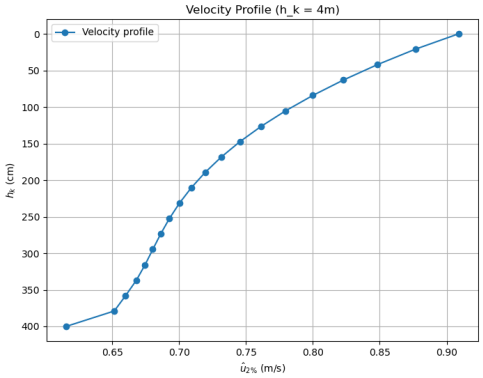

FIGURE 5.5: Velocity profile for SWASH-VEG-10

The modeling of the vegetation is to some extent successful, in terms of stability the model runs smoothly. The model runs successfully with the given input parameters, but the results do not match with the Deltaflume measurements. The vertical velocity profiles are not represented well due to the relative course layering and the effect of layer-averaging, making the proper representation of the near-bed velocity unreliable. The deeper the water gets, the more the averaging gets a significant effect on the results. This implies that vegetation modeling to obtain the accurate near-bed velocities requires a higher vertical resolution. This comes with its own challenges like, numerical stability and computational costs. The effect of the vegetation is also not significant in the modeling, where up to 10% extra attenuation is expected, the model gives a maximum of around 1% extra attenuation capacity, additionally the velocities ($\hat{u}_{2\%}$) are too high in the lower layer in comparison with the measurements.

6 Discussion

6.1 Effect of wave characteristics and waterlevel on near-bed velocities at the toe

The effect of the water level on the wave-driven near-bed velocities at the toe of a dike is significant. The water level plays a crucial role in shaping the near-bed flow velocities at the toe of a dike. At lower water levels, the velocity is typically lower than with higher water levels, induced due to the smaller wave height at lower water levels. The numerical model extends the dataset with extra velocities at other $\frac{H_{m0}}{h_k}$ values. The near-bed velocity component grows until a relative wave height of 0.78, which is the critical number for wave breaking (Thornton and Guza, 1983). The 2% value for the velocity stays relatively constant from this point onward, where the maximum $u_{2\%}$ is around 1.0 ms^{-1}. At lower water levels, the reduced wave height results in a diminished near-bed velocity, corresponding to the principles of wave transformation over shallow depths described by Battjes and Janssen (1978). Conversely, at higher water levels, increased wave energy translates to greater near-bed velocities until the breaking threshold is reached. This is an intuitive conclusion, because the orbital velocities are influenced by wave height, wavelength and water depth (Soulsby, 2006). An important aspect is that the interested velocity field is within the wave base, because the orbital motion becomes negligible at a depth of approximately $0.5 * L_0$. With $h_0 < 0.5 * L_0$ in all the experiments, the orbital motion at the bed is always significant. The observed trends underline the importance of considering water level variability, especially when predicting wave-induced impacts near structures like dikes. At certain water levels, the near-bed velocities reduce in magnitude, which can be beneficial for the dike design.

The wave characteristics also play a role on the resulting near-bed hydrodynamics. In the Deltaflume experiments H_{m0} and T_p are chosen to align with a certain wave steepness, resulting in wave steepness of 0.02 and 0.04. Without vegetation present, shorter waves (higher steepness) result in slightly lower near-bed velocities for the lowest and intermediate water level. This characteristic is confirmed by the numerical modeling. This means waves with a steepness of 0.04 produce lower near-bed velocities than waves with a steepness of 0.02. This can be professed by the study of Dean and Dalrymple (1991), which states that the orbital paths become more elliptical for steeper waves. This shift reduces the horizontal component of the velocity, which is the dominating factor for the near-bed velocity. The stagnation in velocity can be explained. A higher wave power would intuitively lead to a higher orbital velocity. However, a study by Dinh et al. (2023) suggests a frequency dependent dissipation, where the energy dissipation is generally greater in the lower frequency (s_{op} = 0.02) than in the higher frequency (s_{op} = 0.04) range.

Near-bed velocity approximations based on theory and literature were compared to the velocity measurements from the Deltaflume. None of the estimators can predict the near-bed velocity accurately. Due to the presence of a saltmarsh, the wave transformations are more complex and non-linear than expected. Due to the higher non-linearity of the wave transformations the approximations fail to accurately predict the velocities. The non-linear effects include the effect of the saltmarsh cliff, the wave attenuation on a constant horizontal (vegetated) saltmarsh of a certain length and the interaction with reflected waves of the hydraulic structure. Van Gent and van der Werf (2014) is developed to predict near-bed velocities at the toe of a dike, but with a sloping foreshore without a saltmarsh present.

Little to no erosion at the toe of the dike was observed during the Deltaflume experiments, but it was expected as described in earlier studies (Klein Breteler et al., 2024).

Mainly with damaged vegetation, a significant erosion pit was expected at the toe. This indicates that the highest velocity components observed during the tests, do not exceed the critical velocity for the soil and vegetation type. Erosion occurs when the critical velocity (u_{crit}) is exceeded by the wave-driven velocity. The measured velocities do not exceed 1 ms^{-1} in any of the test cases. The numerical model simulations show slightly higher velocities, but not exceeding 1.15 ms^{-1}. This implies that the u_{crit} of the saltmarsh is never exceeded. A study by Schoutens et al. (2022) conducted similar experiments, with simulating wave conditions over a saltmarsh. In this study near-bed velocities reached a maximum of 1.75 ms^{-1}, without significant erosion on the saltmarsh. It should be noted that these velocities are depth-averaged over a depth ranging from 0.15 to 0.35 m, assuming a shallow water velocity profile, this would result in the maximum velocities occurring at the bed. This underpins the sediment stability of saltmarshes against vertical erosion under storm surge conditions

6.2 Effect of vegetation on near-bed flow velocities

Vegetation induces an increased dissipation rate, resulting in a decrease of wave-driven near-bed velocities. This was also found in literature, where the wave attenuation by a saltmarsh is significant, even at the highest water levels and wave conditions (Möller et al., 2014). The effect of the vegetation is clearly depicted in Figure 4.3 for the Deltaflume tests. Both the vegetation with little damage and the vegetation with much damage show a significant reduction in near-bed orbital velocities.Similar to the conclusion reached by Möller et al. (2014), longer waves experience greater attenuation than shorter waves. The research focuses on the near-bed velocities instead of the wave heights as studied by Möller et al., 2014. This result is realistic, because the near-bed velocity is directly proportional to the wave height, but has an inverse relation to the wave period (Airy, 1841).

6.3 Effect of dike slopes on near-bed flow velocities

The effect of the dike slopes varies for each water depth and wave height. As depicted in Figure 5.2. For H_{m0} = 0.75, the velocity decreases when decreasing the dike slope. Velocities are generally lower across all the slopes due to the reduced wave energy that is associated with lower water levels. The decreasing trend represents the dissipation on gentler dike slopes. For the intermediate depth (5.4m) the effect is inverse, the velocity grows when decreasing the dike slope, with a peak at $1:6$. The moderate water levels maximizes wave energy near the toe for a slope of $1:6$. For the highest water level (6.9m), the wave energy is mostly retained due to the greater water depth. Gentler slopes can allow more energy to be retained due to a gradual energy dissipation over a longer distance, reduced wave breaking near the toe. The velocity is mainly depending on water levels combined with the slope. While steeper slopes reflect energy, reducing toe velocities, gentler slopes dissipate energy gradually, causing velocities to increase and peak at moderate slopes before stabilizing at the gentlest slopes. This trend highlights the importance of balancing slope steepness and water levels to manage toe velocities effectively if erosion would be a problem. The amount of reflection can be extracted from the numerical model, but additional modeling is necessary to obtain the amount of reflection.

6.4 ADV measurements in vegetation

The ADV measurements that are conducted are deemed accurate in vegetation. The used filtering techniques by giving a certain threshold for correlation and SNR gave reliable results in terms of velocity signal. The SNR ratio of the measurements were not significantly contaminated by the vegetation present in the flume, it even improved in SNR, requiring less data to be removed due. In terms of correlation the vegetation did add extra uncertainty in the measurements. Due to the addition of vegetation in the measurements, around twice the amount of data had to be filtered out in terms of correlation errors. The vegetation can introduce additional uncertainty in ADV measurements (especially in correlation), the net effect on SNR can be neutral or even beneficial in some conditions due to increased scattering surfaces. With appropriate despiking as and threshold filtering as opposed by Goring and Nikora (2002), the ADV remains reliable even in flows with vegetation at the cost of a higher percentage of invalid or noisy data that must be removed during post-processing.

6.5 Accuracy of the numerical model

The numerical model performs well in predicting wave height evolution over the saltmarsh fo the steep waves ($s_{op} = 0.04$), with maximum errors of 10% deviation of the flume measurements being reasonable. Whereas, in shallow waters the waves with $s_{op} = 0.02$ are predicted well enough. In deeper waters, the wave evolution seems to become inaccurate, this is clearly depicted in the spectral density plots. Some spectra show almost no energy loss at all for the propagating waves over the saltmarsh. Less steep waves have longer wave periods, which have longer wave lengths. Longer wave lengths can be sensitive to numerical dispersion in the model. Numerical dispersion occurs when the model equations approximate the continuous wave equations in a way that artificially shifts or distorts the wave signal (Dean and Dalrymple, 1991). The grid size resolution (dx) might be adequate for the shorter waves, they do not suffice for the longer waves. Longer waves are more spread out over the grid, requiring a finer resolution for properly solving the equations. In terms of velocities, the model is $\approx$ 0.1 ms^{-1} inaccurate, mostly overestimating. The overestimation can be caused because the wave transformation is not modeled exactly right, this is observed in the tables given in the modeling chapter. In most cases, the wave attenuation is underestimated (waves are too high at the toe compared to the observations). The near-bed orbital velocity is directly proportional to the wave height, meaning that if the wave height prediction has a slight error, the near-bed orbital velocity also contains a slight error. The prediction of the velocity for the test without vegetation are accurate or overestimating slightly.

Something to consider is the waves interaction with the bed for spectra with a different wave steepness. As mentioned before, for each water depth two different wave steepnesses were tested. A steeper wave has an increased wave energy and enhanced turbulence in the bottom boundary layer (Scott et al., 2009). This suggests that frictional effects for steeper waves are different from those of less steep waves, requiring adjusted friction coefficients in the numerical model. Adding to this suggestion, the results of the numerical model do not result in significant differences in the wave attenuation capacity when comparing the steeper and the less steep wave, which is the case in the Deltaflume measurements. A study by Zhang et al. (2020) also showed that wave steepness significantly affects the bottom roughness calibration. Steeper waves tend to induce a higher energy dissipation, requiring a reduction in bottom roughness to avoid overestimating the wave height attenuation and velocities. Hence, the friction coefficient for different wave

steepnesses should have a different calibration procedure, this is not conducted due to time constraints. However, the model should not have a different calibration procedure for different wave steepnesses, meaning that the issue is most likely a numerical modeling issue.

The vegetation is implemented as proposed by the SWASH manual, with the vegetation input parameters determined as measured during the Deltaflume experiments (vegetation height, diameter, number of stems and the resulting drag coefficient). The results are shown in Table 5.2, and the model converges worse in terms of wave height attenuation and near-bed orbital velocities when the water depth increases. Most likely the wave dampening effect of the vegetation which get less less pronounced when the water depth increases (Suzuki et al., 2012). The C_d value is determined using the method for irregular waves by Möller et al., 2014. This method works well for the deep water waves, but when the water gets shallower, the method seems to become less accurate (see Table 5.2). This can be caused by how waves interact with the vegetation: waves in shallow water interact differently and with more complex dynamics than waves in deeper waters. In shallow waters the wave-wave interactions are more complex adding extra uncertainty in the numerical modeling. When comparing the models without vegetation with the models with vegetation in terms of velocities, the velocities are higher with vegetation. The opposite would be expected, lowered velocities near the bed. This can be caused due to how the layers are modeled (layer height), the velocities are averaged over a certain depth. Due to the high non-linearity and in-canopy flow in the model, the averaging can induce an unrealistic velocity output. It could also be that the drag coefficient formula by Muller (2022) is not accurate enough for the great range of varying water levels conducted in this study.

6.6 Limitations of this research

The Deltaflume tests are all conducted with a $\frac{H_{m0}}{h_k}$ ratio of 0.5, mainly limited by the maximum wave height of 2m that can be produced in the flume. However, different $\frac{H_{m0}}{h_k}$ velocity measurements could have given a deeper insight on the velocity response. Measurements are more reliable than model results, which cannot be further verified in this case. Also measurements at more points in the flume could have given a broader insight on the velocity profile development over the saltmarsh. The $\frac{H_{m0}}{h_k}$ ratio of 0.5 was chosen because at this ratio the effect of the vegetation would become more pronounced. But as shown in the numerical modeling of different ratios, measurements of higher ratios could have resulted in interesting insights.

In the numerical modeling, some choices had to be made to make the model workable. Some choices do not necessarily align with other studies. E.g. a maximum Courant Number of 0.5 is advised for high and non-linear waves by The SWASH team, 2024. But this caused the model to be less robust and crash, giving a timestep error. A too small timestep would have cost a lot of extra computational time. Also the maximum number of layers is a limitations, more layers would be desirable to obtain a better representation of the near-bed velocities. This can be achieved by further improving the model and trying different numerical schemes. Another limitation is the depth-averaging of the velocity per layer, e.g. taking the velocity in the lowest grid cell could be a solution. Another addition is that the effect of the walls in the flume could potentially have an effect on the wave transformations, this is not accounted for in the numerical model.

6.7 Implications for implementing a Living Dike as coastal protection

The ADV data clearly shows a decrease in near-bed velocities at the toe of a dike due to the vegetation that is present on the saltmarsh. This reduction in velocities is around 52%, a significant amount. The occurring velocities are way smaller than the critical velocities for grass covered clay, implying scour at the toe of a dike is not a risk for dikes fronted with a saltmarsh. Even in highest storm conditions, no significant erosion has occurred (Klein Breteler et al., 2024). The research also shows that maximum velocities occur around $\frac{H_{m0}}{h_k}$ values of 0.8, generally agreeing with 0.78 as found by Thornton and Guza (1983). This shows that after waves have broken, a reduction in near-bed orbital velocity is present at the toe of the dike, reducing the risk of erosion.

The finding that the critical velocity ($u_{crit} > \hat{u}_{2\%}$) was never exceeded and no erosion was observed, highlights the effectiveness of the saltmarsh in attenuating wave energy and near-bed orbital velocities and protecting the dike toe. This confirms the stability of the system under the storm conditions and reduces the risk of erosion-driven damage. It supports the use of saltmarshes as a nature-based solution, demonstrating their value in hybrid flood defense designs. The results also provide valuable data for further validating numerical models and encourage sustainable practices like saltmarsh restoration and incorporation in dike design. Overall, this study reinforces the protective and ecological benefits of incorporating saltmarshes into coastal management strategies.

7 Conclusions

The goal of of this research is to assess the near-bed orbital velocities near the toe of a dike based on recent Deltaflume experiments and numerical modeling under varying storm conditions. This conclusion answers the research questions and presents the key findings in this research:

7.1 What are the characteristics of wave-driven near-bed velocities during storm conditions at the transition zone between a saltmarsh and coastal dike?

RQ1a: What is the effect of different water levels and wave characteristics?

Steeper waves lead to higher near-bed velocities compared to less steep waves in vegetation, due to the elliptical orbital paths that reduce the horizontal velocity component. In the absence of vegetation, the nuance is less distinct, with minimal difference observed. This is based on both Deltaflume experiments and additional the numerical simulations. At the toe of a dike, the near-bed velocity peaks at around 0.85 ms^{-1} for offshore wave heights of H_{m0} = 2.0 m. Mainly the $\frac{H_{m0}}{h_k}$ ratio plays a significant role in the occurring near-bed velocities. The maximum near-bed orbital velocities occur around $\frac{H_{m0}}{h_k}$ of 0.8, which is assumed to be at the ratio of wave breaking.

RQ1b: What is the relation between standing saltmarsh vegetation and flow velocities?

Vegetation increases energy dissipation, reducing the near-bed velocities. Longer waves are attenuated more by vegetation than shorter waves. A reduction in near-bed velocities of 52% is observed for offshore waves up to $H_{m0,0}$ = 2.0m for the fully standing vegetation. For partly damaged vegetation, the near-bed velocity reduction decreases with 29% to 23%. Numerical modeling confirms the non-linear velocity profile with vegetation present, but overestimates due to the depth-averaging over the layers, indicating the complex interaction between vegetation and wave energy dissipation.

RQ1c: What is the effect of different dike configurations?

The dike slope can significantly influence the near-bed velocity for different water levels, where gentler slopes dissipate more energy over longer distances, increasing near-bed velocities under moderate water levels, potentially due to rundown. Steeper slopes reflect more wave energy, which could cause the reduction in velocities. The water level also plays an important role. Due to an increase or decrease in water level, the velocity profile changes. Numerical simulations show a clear distinction in the effect of different water levels and wave heights on varying dikes lopes, but further research is necessary to get an exact understanding.

7.2 How effectively can the near-bed velocities at the transition zone between a saltmarsh and a coastal dike be captured and modeled?

RQ2a: How well can an ADV measure near-bed orbital velocities in vegetation?

The ADV positioned inside the saltmarsh vegetation generally measured the local orbital velocities accurately. In terms of SNR and Correlation values, more filtering is necessary

than without the vegetation present. In terms of SNR, the data improves due to the added increased scattering surfaces added by the vegetation. In terms the of correlation the data decreases in quality due to the interference of vegetation with the measurement probes. The standard outlier removal algorithm, identifying outliers as values > 2 times the standard deviations performs pretty well and results in reliable data.

RQ2b: How accurately can a phase-resolving non-hydrostatic numerical model simulate near-bed orbital velocities in environments with and without vegetation?

Due to complex bathymetry and varying water levels, the numerical modeling of all the scenarios is difficult. For the current model setup, changing water depth and wave parameters causes numerical instability. Without vegetation, the numerical model predicts with sufficient accuracy, but including vegetation overestimates the near-bed velocities significantly. This can be due to various cases, e.g. not enough vertical grid resolution, wrong Courant number limits or a wrong representation of the drag coefficient. This must be explored and calibrated in further research.

Final conclusion

The velocities vary significantly based on water levels, wave steepness and the presence of vegetation. Higher water levels allow higher waves to reach the dike, resulting in greater near bed velocities. Higher water levels generally result in higher near-bed velocities due to possible development of higher waves. Numerical simulations confirms that the maximum near-bed velocity is governed by the $\frac{H_{m0}}{h_k}$ ratio . The highest measured near-bed velocities in the Deltaflume are 0.85 ms^{-1} and 1 ms^{-1} in the SWASH numerical model. These velocities are far lower than the critical velocities for erosion of clay covered with grass. Erosion at the toe of the dike is not observed in the tests, nor is expected to happen in circumstances as tested in this research. The presence of vegetation greatly reduces the near-bed velocities, even in more broken state after several hours of testing. Maximum near-bed velocities at the toe which were measured and confirmed additional numerical simulations did not exceed 1.0 ms^{-1}, even under extreme wave conditions of H_{m0} = 2.0 m. The little to zero erosion at the toe of the dike at the end of the Deltaflume experiments, demonstrate the stability of the saltmarsh at that location and nuance the risk of erosion-driven damage. It supports the use of saltmarshes as a nature-based solution for flood defenses and demonstrates their value in hybrid flood defense designs.

8 Recommendations

8.1 Extend dataset

Conducting more tests with varying $\frac{H_{m0}}{h_k}$ ratios can confirm whether the numerical model is accurate. This also allows calibration for different $\frac{H_{m0}}{h_k}$ ratios. When a numerical model is more robust and can simulate all the water levels, an extension of the numerical simulations can be made. The evolution of $\frac{H_{m0}}{h_k}$ with vegetation present would be a valuable insight, but also the response of the velocities in comparison to the dike slopes can be altered due to vegetation presence. Also, more simulations can be simulated to extend each of the plotted figures concerning the dike slopes or the $\frac{H_{m0}}{h_k}$ ratios.

The extension of the dataset can also extend the understanding of the near-orbital velocity interaction with the vegetation. Different $\frac{H_{m0}}{h_k}$ ratios can be tested and the frequency dependent dissipation can be addressed more extensively.

8.2 Improving numerical model

The numerical model can be improved, especially to solve less steep waves. Numerical dispersion plays a role due to the limited horizontal step or time step. The improved models will require a lot more computational effort to solve, needing computational clusters to be solved efficiently. The dataset of the ADV measurements can be used for the calibration procedure, also the Manning roughness coefficient works properly for modeling the bottom roughness. The depth-averaging per layer would become more accurate if the resolution gets higher, it is recommended to improve the resolution whilst maintaining model stability. Other additions would be acquiring a higher resolution in depth of the model, allowing for better wave transformation over the saltmarsh. Also different breaker parameters could represent the interaction of waves with the saltmarsh in a better way. Another addition could be an improved turbulence model to address higher resolution turbulence effects. In this study, a difference in the interaction with different dike slopes was found from the numerical model results. However, the exact processes behind these results are still unclear. Further investigation should be carried out on for example, the reflection, overtopping or wave breaking on the slope as calculated by the numerical model to get a clearer picture of the exact processes at the toe of the dike for different dike slopes.

8.3 Vegetation modeling

The SWASH models including vegetation clearly overestimate the near-bed orbital velocities, due to the lower resolution of the vertical grid. The depth-averaging of the layers results in a too coarse resolution. In order to accurately model the velocities a higher vertical resolution needs to be applied. This can either be obtained by applying a logarithmic layer distribution, or increasing the amount of layers of the model. Both bringing their own numerical challenges and limitations. The depth-averaging of the velocities can be a limitation of the SWASH model for the modeling of this case. Other types of models can also be explored to see whether the near-bed orbital velocity is represented in a more realistic way, instead of averaging over the depth of a horizontal layer (e.g. Open Foam).

8.4 Erosion theories

In this study, the maximum near-bed velocities at the toe were quantified. However, the direct link with erosion due to shear is still missing. It is recommended to assess the effect of the velocities on the bed-shear stresses and compare this to existing erosion theories, to obtain an understanding in what scenarios erosion would be a potential thread.

References

Airy, G. (1841). Tides and waves (MixedSciences).

Arias, P. A., Bellouin, N., Coppola, E., Jones, R. G., Krinner, G., & Marotzke, J. (2021, June). Technical Summary. In *Climate change 2021 – the physical science basis* (pp. 33–144). Cambridge University Press. https://doi.org/10.1017/9781009157896.002

Barbier, E. B., Hacker, S. D., Kennedy, C., Koch, E. W., Stier, A. C., & Silliman, B. R. (2011, May). The value of estuarine and coastal ecosystem services. https://doi.org/10.1890/10-1510.1

Battjes, J. A., & Janssen, J. P. F. M. (1978). Energy loss and set-up due to breaking random waves ENERGY LOSS AND SET-UP DUE TO BREAKING OF RANDOM WAVES 1) 2). https://doi.org/10.9753/icce.v16

Beudin, A., Kalra, T. S., Ganju, N. K., & Warner, J. C. (2017). Development of a coupled wave-flow-vegetation interaction model. *Computers and Geosciences*, *100*, 76–86. https://doi.org/10.1016/j.cageo.2016.12.010

Bosboom, J., & Stive, M. J. F. (2023, November). *Coastal Dynamics* (tech. rep.). Delft University of Technology. Delft. https://LibreTexts.org

Cohen-Shacham, E., Walters, G., Janzen, C., & Maginnis, S. (2016, August). *Nature-based solutions to address global societal challenges*. IUCN International Union for Conservation of Nature. https://doi.org/https://doi.org/10.2305/IUCN.CH.2016.13.en

de Vriend, H., van Koningsveld, M., & Aarninkhof, S. (2014). 'Building with nature': The new Dutch approach to coastal and river works. *Proceedings of the Institution of Civil Engineers: Civil Engineering*, *167*(1), 18–24. https://doi.org/10.1680/cien.13.00003

Dean, R. G., & Dalrymple, R. A. (1991, January). *Water Wave Mechanics for Engineers and Scientists* (Vol. 2). WORLD SCIENTIFIC. https://doi.org/10.1142/1232

Dinh, Q. C., Nguyen, Q. T., Ho, D. D., & Mai, C. T. (2023). Effects of bottom roughness on wave transmission across a submerged reef. *Frontiers in Marine Science*, *10*. https://doi.org/10.3389/fmars.2023.1113195

Engineering Toolbox. (2004). Manning's Roughness Coefficients.

Goring, D. G., & Nikora, V. I. (2002). Despiking Acoustic Doppler Velocimeter Data. https://doi.org/10.1061/ASCE0733-94292002128:1117

Hashim, R., Roy, C., Motamedi, S., Shamshirband, S., & Petković, D. (2016, July). Selection of climatic parameters affecting wave height prediction using an enhanced Takagi-Sugeno-based fuzzy methodology. https://doi.org/10.1016/j.rser.2016.01.098

Hoffmans, G., & Verheij, H. (1997). *Scour Manual* (tech. rep.).

Holthuijsen, L. H. (2007, January). *Waves in Oceanic and Coastal Waters*. Cambridge University Press. https://doi.org/10.1017/CBO9780511618536

Ifuku, M., & Hayashi, H. (1998). Development of Eelgrass (Zostera marina) bed utilizing sand drift control mats. *Coastal engineering journal*, *40*(3), 223–239. https://cir.nii.ac.jp/crid/1573668924496879616.bib?lang=en

Jadhav, R. S., Chen, Q., & Smith, J. M. (2013). Spectral distribution of wave energy dissipation by salt marsh vegetation. *Coastal Engineering*, *77*, 99–107. https://doi.org/10.1016/j.coastaleng.2013.02.013

Johnson, H. K., & Kofoed-Hansen, H. (2000). Influence of Bottom Friction on Sea Surface Roughness and Its Impact on Shallow Water Wind Wave Modeling. https://doi.org/https://doi.org/10.1175/1520-0485(2000)030<1743:IOBFOS>2.0.CO;2

Kirwan, M. L., & Megonigal, J. P. (2013). Tidal wetland stability in the face of human impacts and sea-level rise. https://doi.org/10.1038/nature12856

Klein Breteler, M., Willemsen, P., & van Bergeijk, V. (2024, May). *CONCEPT Bijdrage van kweldervegetatie aan het waterkeringssysteem* (tech. rep.). Deltares. Delft.

Lane, S. N., Biron, P. M., Bradbrook, K. F., Butler, J. B., Chandler, J. H., Crowell, M. D., Mclelland, S. J., Richards, K. S., & Roy, A. G. (1998). Three-dimensional measurement of river channel flow processes using acoustic doppler velocimetry. *Earth Surface Processes and Landforms*, *23*(13), 1247–1267. https://doi.org/10.1002/(SICI)1096-9837(199812)23:13<1247::AID-ESP930>3.0.CO;2-D

Lomonaco, P. (1997). Pipeline rock cover damage assessment. https://doi.org/10.13140/RG.2.1.3586.7684

Losada, I. J., Maza, M., & Lara, J. L. (2016). A new formulation for vegetation-induced damping under combined waves and currents. *Coastal Engineering*, *107*, 1–13. https://doi.org/10.1016/j.coastaleng.2015.09.011

Mai, C., Pilarczyk, K., & van Gelder, P. (2006). *Foreshore erosion and scour induced failures of sea dikes* (tech. rep.). https://doi.org/https://hdl.handle.net/20.500.11970/100047

Marijnissen, R., Esselink, P., Kok, M., Kroeze, C., & van Loon-Steensma, J. M. (2020). How natural processes contribute to flood protection - A sustainable adaptation scheme for a wide green dike. *Science of the Total Environment*, *739*. https://doi.org/10.1016/j.scitotenv.2020.139698

Möller, I., Kudella, M., Rupprecht, F., Spencer, T., Paul, M., Van Wesenbeeck, B. K., Wolters, G., Jensen, K., Bouma, T. J., Miranda-Lange, M., & Schimmels, S. (2014). Wave attenuation over coastal salt marshes under storm surge conditions. *Nature Geoscience*, *7*(10), 727–731. https://doi.org/10.1038/NGEO2251

Monteban, D. (2016). *Numerical modelling of wave agitation in ports and access channels* [Doctoral dissertation].

Morris, J. T., Sundareshwar, P. V., Nietch, C. T., Kjerfve, B., & Cahoon, D. R. (2002). *Responses of Coastal Wetlands to Rising Sea Level* (tech. rep. No. 10).

Muller, J. (2022). Stability of saltmarshes under storm conditions - Ph.D Qualifier Research Report.

Nammuni Nee Krohn, J. (2009). *FLOW VELOCITY AT RUBBLE MOUND BREAKWATER TOES* [Doctoral dissertation, TU Delft]. https://repository.tudelft.nl/record/uuid:fe20c5e2-051e-45fe-aaa5-aac0bb113e18

Nortek. (2024). *Sample 3D velocity at up to 64 Hz for small-scale research in coastal areas* (tech. rep.).

Nortek AS. (2018). *The Comprehensive Manuel for Velocimeters* (tech. rep.). Nortek AS. Rud.

Oppenheimer, M., Glavovic, B. C., Hinkel, J., van de Wal, R., & Magnan, A. K. (2022, February). Sea Level Rise and Implications for Low-Lying Islands, Coasts and Communities. In *The ocean and cryosphere in a changing climate* (pp. 321–446). Cambridge University Press. https://doi.org/10.1017/9781009157964.006

Piontkowitz, T., & Chistensen, K. (2012). *EroGRASS Failure of Grass Cover Layers at Seaward and Shoreward Dike Sloppes - Performance, Results and Conclisions* - (tech. rep.). HydralabIII.

Reis, R. A., Pires-Silva, A. A., Fortes, C. J., & Suzuki, T. (2020). Experiences with SWASH on modelling wave propagation over vegetation: Comparisons with lab and field data. *Journal of Integrated Coastal Zone Management*, *20*(2), 145–150. https://doi.org/10.5894/RGCI-N303

Schoutens, K., Stoorvogel, M., van den Berg, M., van den Hoven, K., Bouma, T. J., Aarninkhof, S., Herman, P. M., van Loon-Steensma, J. M., Meire, P., Schoelynck, J., Peeters, P., &

Temmerman, S. (2022). Stability of a Tidal Marsh Under Very High Flow Velocities and Implications for Nature-Based Flood Defense. *Frontiers in Marine Science*, *9*. https://doi.org/10.3389/fmars.2022.920480

Schüttrumpf, H., & Oumeraci, H. (2005). Layer thicknesses and velocities of wave overtopping flow at seadikes. *Coastal Engineering*, *52*(6), 473–495. https://doi.org/10.1016/j.coastaleng.2005.02.002

Scott, N. V., Hsu, T. J., & Cox, D. (2009). Steep wave, turbulence, and sediment concentration statistics beneath a breaking wave field and their implications for sediment transport. *Continental Shelf Research*, *29*(20), 2303–2317. https://doi.org/10.1016/j.csr.2009.09.008

Simarro, G. (2024). Influence of Bed Variations on Linear Wave Propagation beyond the Mild Slope Condition. *Journal of Marine Science and Engineering*, *12*(9). https://doi.org/10.3390/jmse12091652

Singh, A. K. (2020). Coastal Agriculture and Future Challenges. https://doi.org/10.1007/978-981-15-4294-7{_}5

Soulsby, R. L. (2006). *Simplified calculation of wave orbital velocities* (tech. rep.).

Stelling, G., & Zijlema, M. (2003). An accurate and efficient finite-difference algorithm for non-hydrostatic free-surface flow with application to wave propagation. *International Journal for Numerical Methods in Fluids*, *43*(1), 1–23. https://doi.org/10.1002/fld.595

Suzuki, T., Zijlema, M., Burger, B., Meijer, M. C., & Narayan, S. (2012). Wave dissipation by vegetation with layer schematization in SWAN. *Coastal Engineering*, *59*(1), 64–71. https://doi.org/10.1016/j.coastaleng.2011.07.006

The SWASH team. (2024). SWASH user manual 10.05a.

Thornton, E. B., & Guza, R. T. (1983). Transformation of wave height distribution. *Journal of Geophysical Research*, *88*(C10), 5925–5938. https://doi.org/10.1029/JC088iC10p05925

Townend, I., Fletcher, C., Knappen, M., & Rossington, K. (2011, December). A review of salt marsh dynamics. https://doi.org/10.1111/j.1747-6593.2010.00243.x

van Rijn, L. C. (2023). *Local scour near structures* (tech. rep.). www.leovanrijn-sediment.com

van Veelen, T. J., Karunarathna, H., & Reeve, D. E. (2021, March). *Modelling wave attenuation by quasi-flexible coastal vegetation* (tech. rep.). Elsevier B.V. https://doi.org/10.1016/j.coastaleng.2020.103820

Van Der Meer, J. W., Janssen, J. P. F. M., Van Der Meer, J. W., & Janssen, J. P. F. M. (1994). *Wave run-up and wave overtopping at dikes and revetments* (tech. rep. No. 485).

Van der Meer, J. W. (2021). Rock Armour Slope Stability under Wave Attack; the Van der Meer Formula revisited. *Journal of Coastal and Hydraulic Structures*. https://doi.org/10.48438/jchs.2021.0008

Van Gent, M. R., & van der Werf, I. M. (2014). Rock toe stability of rubble mound breakwaters. *Coastal Engineering*, *83*, 166–176. https://doi.org/10.1016/j.coastaleng.2013.10.012

Vuik, V., Jonkman, S. N., Borsje, B. W., & Suzuki, T. (2016). Nature-based flood protection: The efficiency of vegetated foreshores for reducing wave loads on coastal dikes. *Coastal Engineering*, *116*, 42–56. https://doi.org/10.1016/j.coastaleng.2016.06.001

Wallast, I., & Gent, M. R. A. v. (2003). STABILITY OF NEAR-BED STRUCTURES UNDER WAVES AND CURRENTS, 1744–1756. https://doi.org/10.1142/9789812791306{_}0147

Wang, X. c., Xin, P., Zhou, Z., & Zhang, F. x. (2023). A systematic review of morphological models of salt marshes. *Water Science and Engineering*, *16*(4), 313–323. https://doi.org/10.1016/j.wse.2023.08.006

Welch, P. D. (1967). *The Use of Fast Fourier Transform for the Estimation of Power Spectra: A Method Based on Time Aver. aging Over Short, Modified Periodograms Ik(fn) =-I A h (%) [a k* (tech. rep. No. 2).

Yager, W. C. (1960). Open channel hydraulics. *Journal of the Franklin Institute*, *270*(1), 59. https://doi.org/10.1016/0016-0032(60)90908-X

Zhang, N., Zhang, Q., Wang, K. H., Zou, G., Jiang, X., Yang, A., & Li, Y. (2020). Numerical simulation of wave overtopping on breakwater with an armor layer of accropode using SWASH model. *Water (Switzerland)*, *12*(2). https://doi.org/10.3390/w12020386

Zijlema, M., Stelling, G., & Smit, P. (2011). SWASH: An operational public domain code for simulating wave fields and rapidly varied flows in coastal waters. *Coastal Engineering*, *58*(10), 992–1012. https://doi.org/10.1016/j.coastaleng.2011.05.015

Zwanenburg, C., de Bruijn, H., & van Vliet, L. (2011). *Impact rapid decrease water level* (tech. rep.). https://www.stowa.nl/deltafacts/waterveiligheid/delta-facts-english-versions/impact-rapid-decrease-water-level#1696

A Full Deltaflume test program

TABLE A.1: Experiment program input for wave gauge in Deltaflume

Experiment no.	**h [m]**	h_k **[m]**	H_{m0} **[m]**	T_p **[s]**	s_{op} **[-]**	L_g **[m]**
SM-01	4.40	1.50	0.75	3.47	0.040	12
SM-02	4.40	1.50	0.75	4.90	0.020	20
SM-03	5.40	2.50	1.20	4.39	0.040	18
SM-04	5.40	2.50	1.20	6.20	0.020	29
SM-05	4.40	1.50	0.75	3.47	0.040	12
SM-06	4.40	1.50	0.75	4.90	0.020	12
SM-07	4.40	1.50	0.75	3.47	0.040	18
SM-08	4.40	1.50	0.75	4.90	0.020	18
SM-09	5.40	2.50	1.20	4.39	0.040	20
SM-10	4.90	2.00	0.91	6.20	0.015	26
SM-11	5.40	2.50	1.20	6.20	0.020	29
SM-12	6.90	4.00	2.00	8.01	0.020	48
SM-13	6.90	4.00	2.00	5.66	0.040	32
SM-14	6.90	4.00	2.00	8.01	0.020	48
SM-15	6.90	4.00	2.00	5.66	0.040	32
SM-16	4.40	1.50	0.75	3.47	0.040	12
SM-17	4.40	1.50	0.75	4.90	0.020	20
SM-18	5.40	2.50	1.20	4.39	0.040	18
SM-19	5.40	2.50	1.20	6.20	0.020	29
SM-20	4.40	1.50	0.75	3.47	0.040	12
SM-21	4.40	1.50	0.75	4.90	0.020	18
SM-22	4.40	1.50	0.75	3.47	0.040	12
SM-23	4.40	1.50	0.75	4.90	0.020	18
SM-24	5.40	2.50	1.20	4.39	0.040	20
SM-25	5.40	2.50	1.20	6.20	0.020	29
SM-26	6.90	4.00	2.00	8.01	0.020	48
SM-27	6.90	4.00	2.00	5.66	0.040	32
SM-28	6.90	4.00	2.00	8.01	0.020	48
SM-29	6.90	4.00	2.00	5.66	0.040	32
SM-30	6.90	4.00	2.00	5.66	0.040	32
SM-31	6.90	4.00	2.00	8.01	0.020	48
SM-32	5.40	2.50	1.20	4.39	0.040	20
SM-33	5.40	2.50	1.20	6.20	0.020	29
SM-34	5.40	2.50	1.20	4.39	0.040	
SM-35	5.40	2.50	1.20	5.06	0.030	
SM-36	4.40	1.50	0.75	3.47	0.040	12
SM-37	4.40	1.50	0.75	4.90	0.020	18
SM-38	4.40	1.50	0.75	3.47	0.040	
SM-39	4.40	1.50	0.75	4.00	0.030	

B SNR of all tests

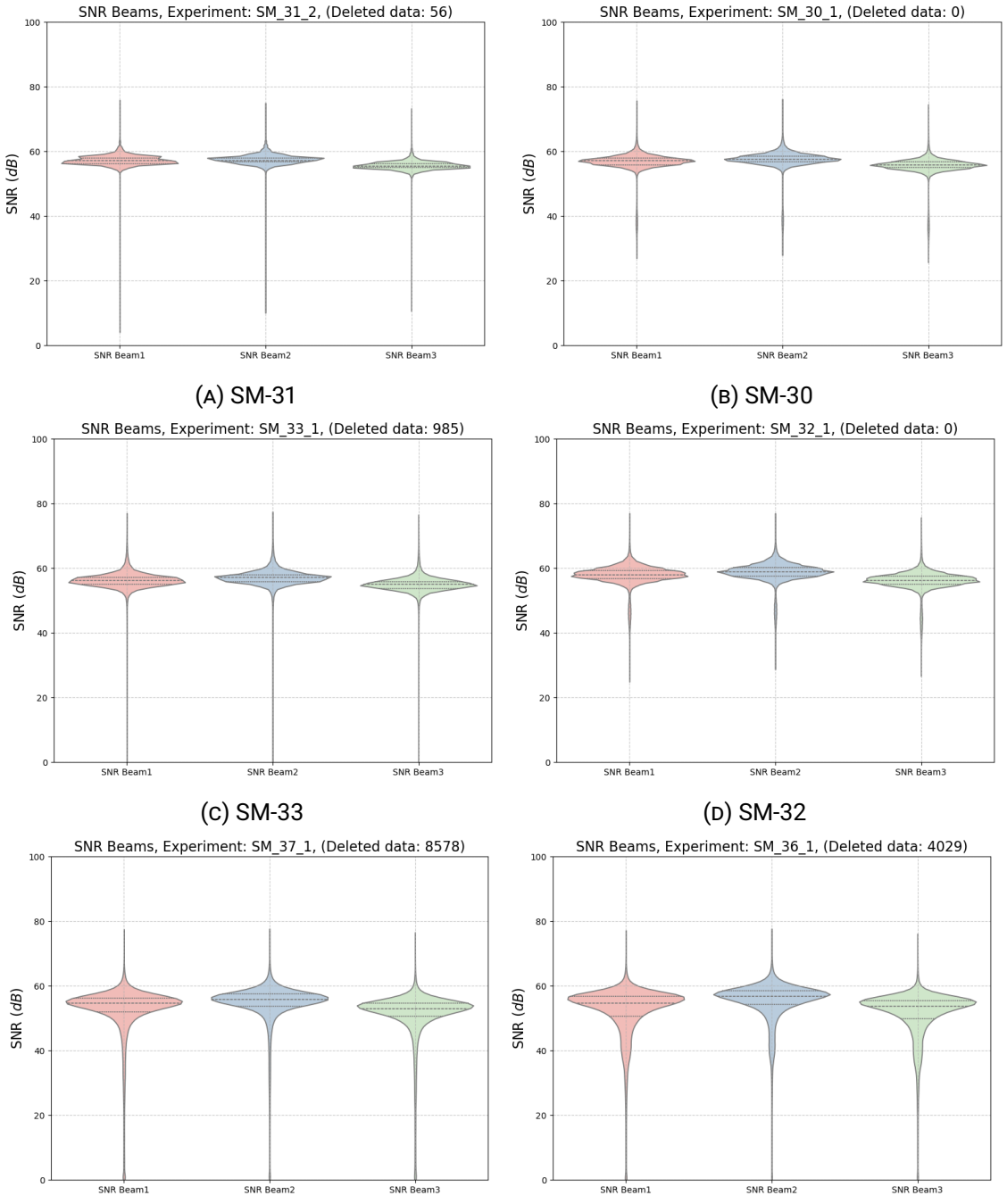

(A) SM-31 (B) SM-30

(C) SM-33 (D) SM-32

(E) SM-37 (F) SM-36

FIGURE B.1: SNR of all Deltaflume experiments without vegetation

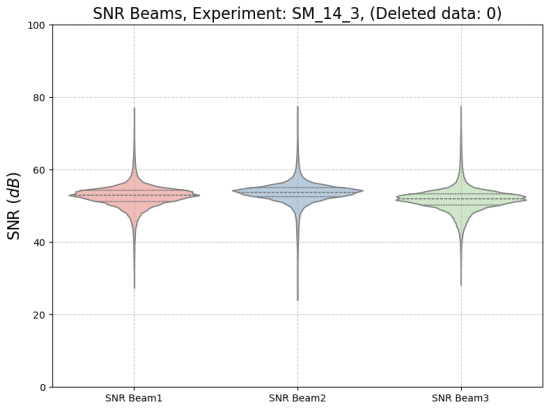

(A) SM-14

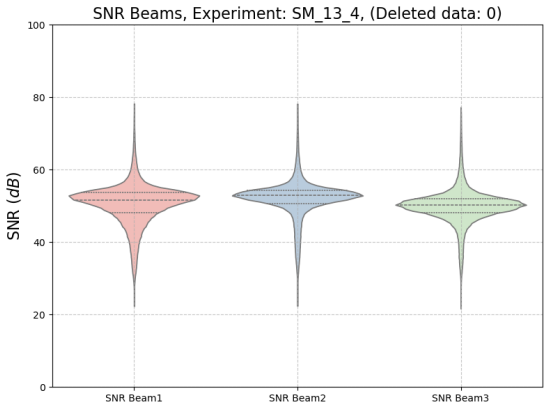

(B) SM-13

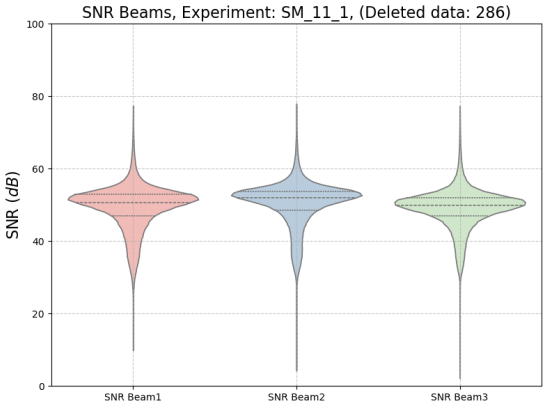

(C) SM-11

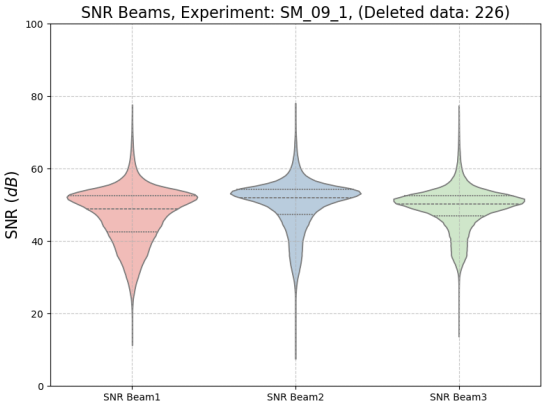

(D) SM-09

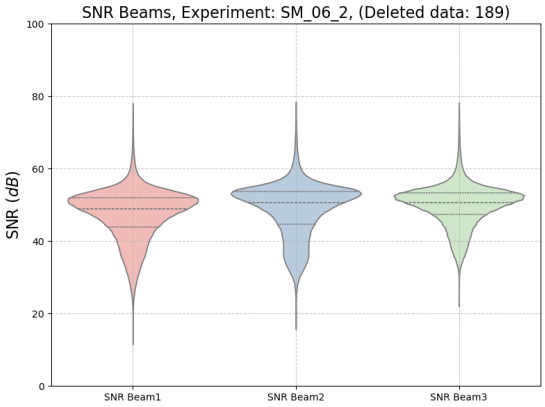

(E) SM-06

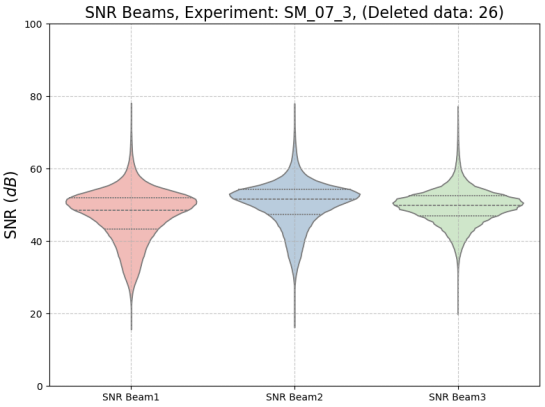

(F) SM-07

FIGURE B.2: SNR of all Deltaflume experiments with damaged vegetation

(A) SM-28

(B) SM-27

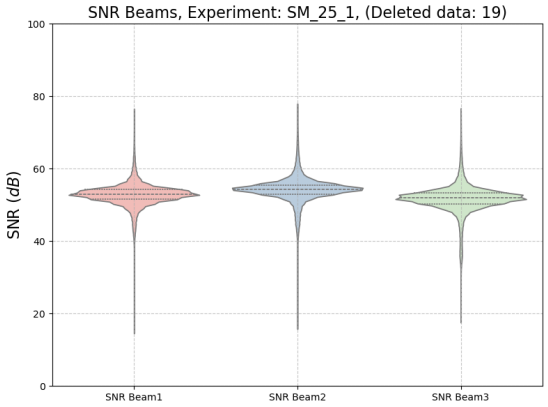

(C) SM-25

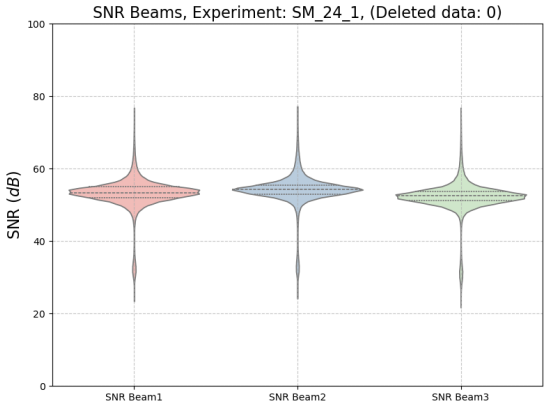

(D) SM-24

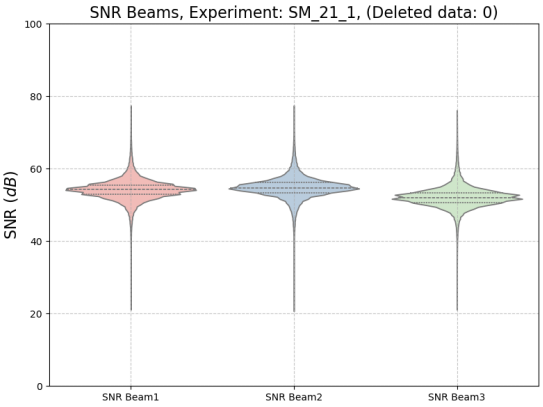

(E) SM-21

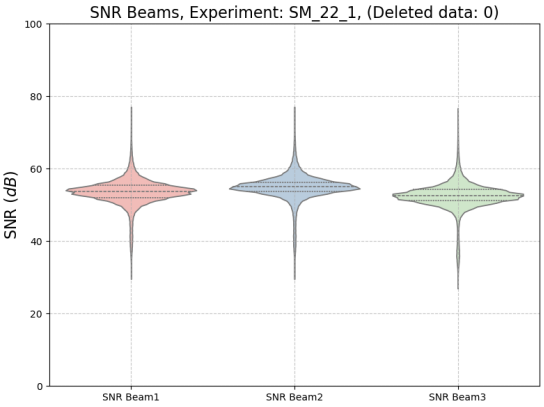

(F) SM-22

FIGURE B.3: SNR of all Deltaflume experiments with undamaged vegetation

C Correlation of all tests

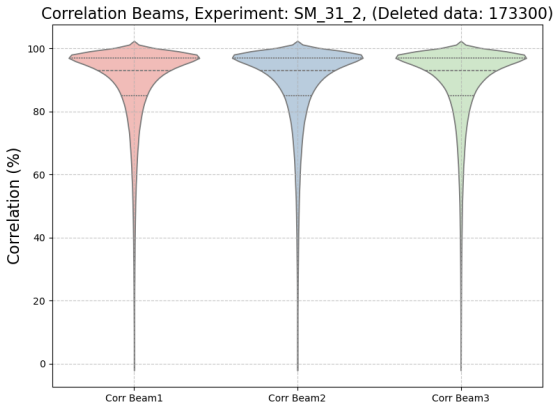

(A) SM-31

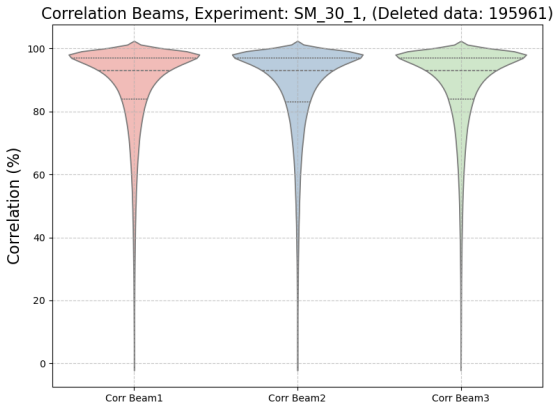

(B) SM-30

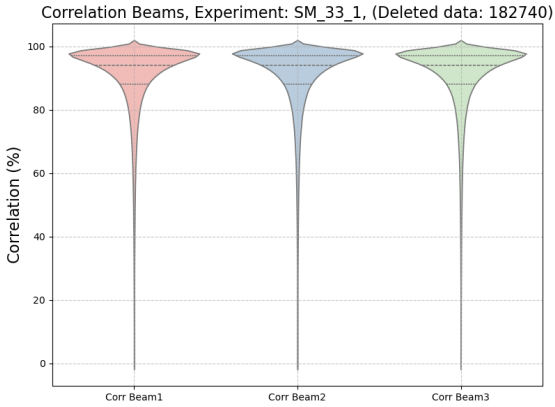

(C) SM-33

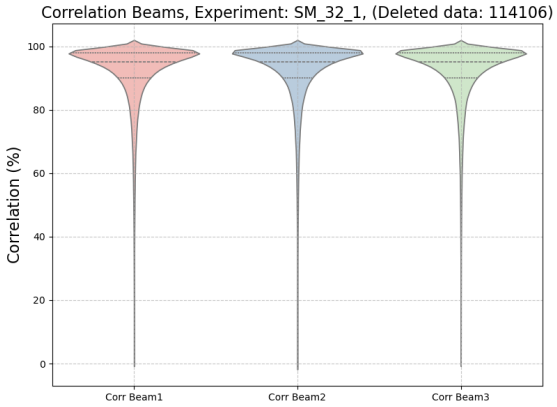

(D) SM-32

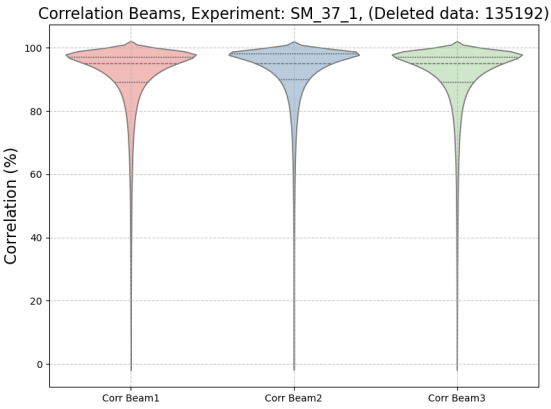

(E) SM-37

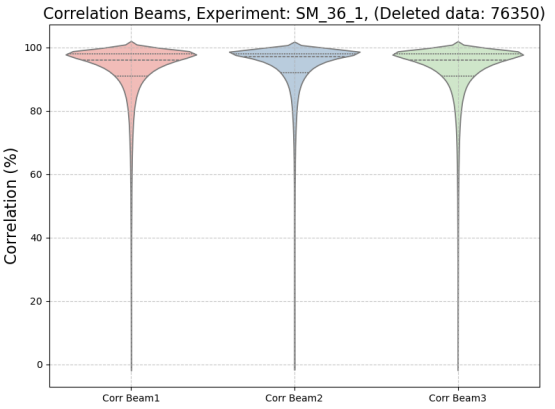

(F) SM-36

FIGURE C.1: Correlation of all Deltaflume experiments without vegetation

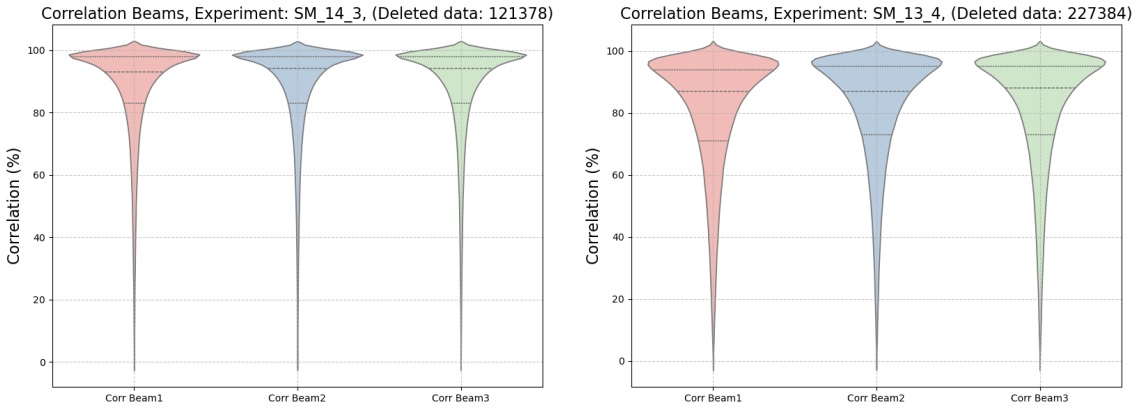

(A) SM-14

(B) SM-13

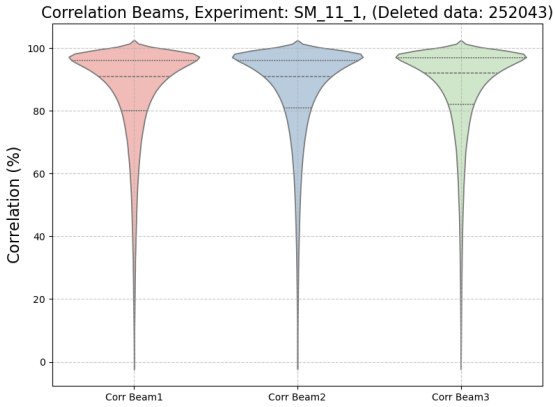

(C) SM-11

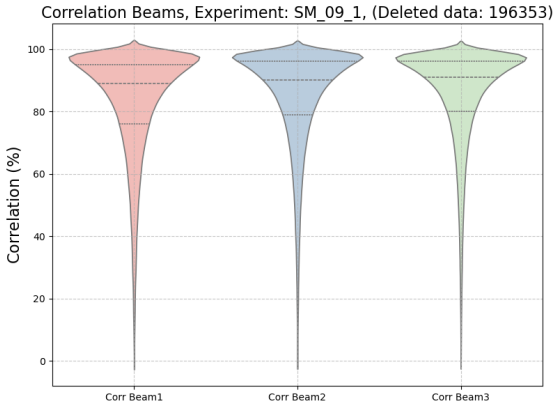

(D) SM-09

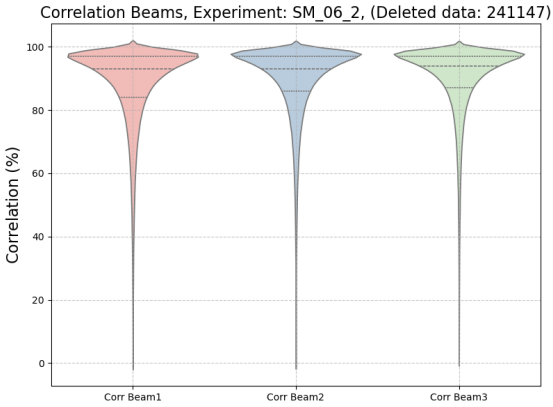

(E) SM-06

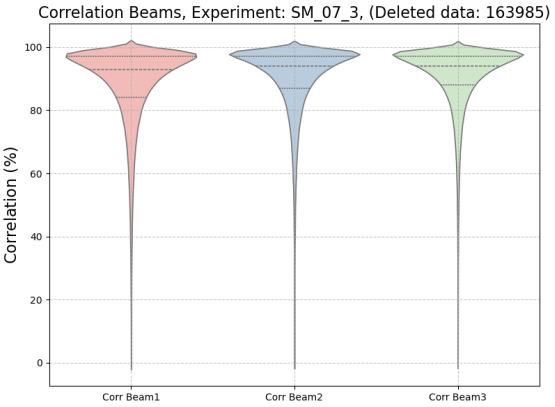

(F) SM-07

FIGURE C.2: Correlation of all Deltaflume experiments with damaged vegetation

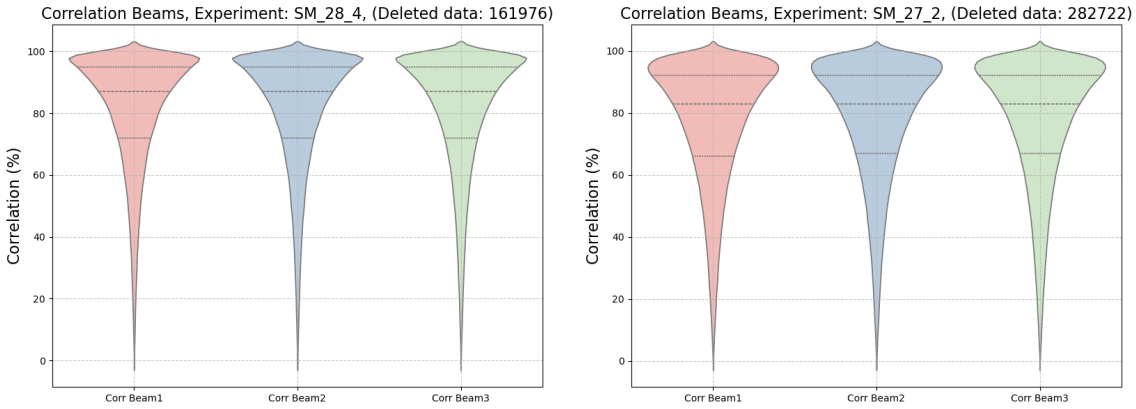

(A) SM-28

(B) SM-27

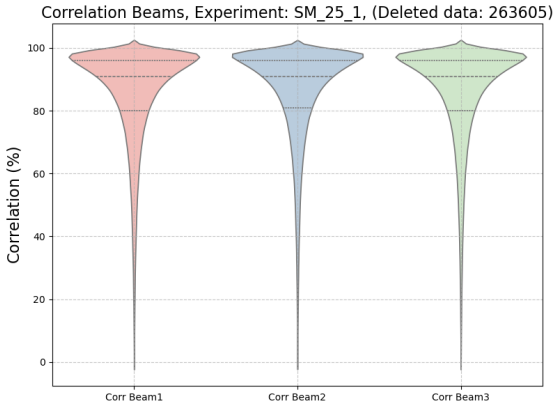

(C) SM-25

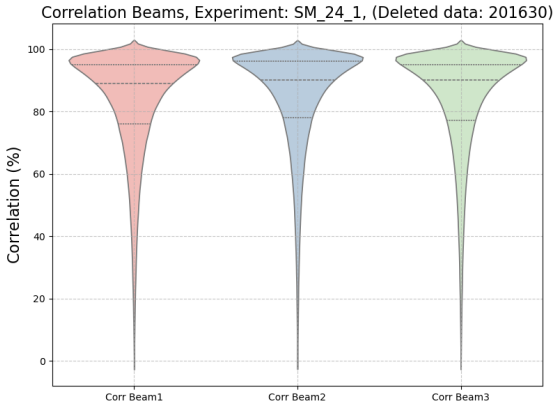

(D) SM-24

(E) SM-21

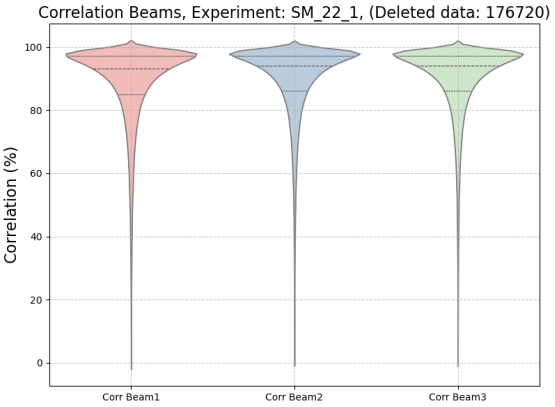

(F) SM-22

FIGURE C.3: Correlation of all Deltaflume experiments with undamaged vegetation

D SWASH numerical model details

The equations used in the SWASH model consisting of the continuity equation, the momentum equation and the vertical momentum equation:

Continuity equation (Mass conservation)

$$\frac{\partial \eta}{\partial t}\frac{\partial}{\partial x}((h+\eta)\bar{u}) = 0 \tag{26}$$

Where η is the free surface elevation, h is the water depth, $\bar{u}$ is the depth-averaged horizontal velocity, t is time and x is the horizontal coordinate.

Momentum equation (Nonhydrostatic Navier-Stokes equations)

Where g is the gravitational acceleration, ρ is the water density, $\bar{p}_{nh}$ is the depth-averaged nonhydrostatic pressure.

$$\frac{\partial \bar{u}}{\partial t} + \bar{u}\frac{\partial \bar{u}}{\partial x} + g\frac{\partial \eta}{\partial x} + \frac{1}{\rho}\frac{\partial \bar{p}_{nh}}{\partial x} = \text{friction + turbulence + other forces} \tag{27}$$

Where w is the vertical velocity, z is the vertical coordinate and p_{nh} is the nonhydrostatic pressure term.

Vertical momentum equation

$$\frac{\partial w}{\partial t} + \bar{u}\frac{\partial w}{\partial x} + w\frac{\partial w}{\partial z} + \frac{1}{\rho}\frac{\partial p_{nh}}{\partial z} = -g \tag{28}$$

E $\frac{H_s}{h_k}$ ratio model parameters

Water depth		Wave properties				Ratios	
h [m]	h_k [m]	H_s [m]	H_{toe}	T_p [m]	s_op [-]	$\frac{H_{m0}}{h_k}$ [-]	$\frac{H_{m0}}{h_k}$ [-]
4.40	1.50	0.75	0.55	3.47	0.04	0.50	0.37
4.90	2.00	0.75	0.59	3.47	0.04	0.38	0.30
5.40	2.50	0.75	0.62	3.47	0.04	0.30	0.25
6.15	3.25	0.75	0.62	3.47	0.04	0.23	0.19
6.90	4.00	0.75	0.62	3.47	0.04	0.19	0.16
4.40	1.50	1.00	0.68	4.00	0.04	0.67	0.45
4.90	2.00	1.00	0.78	4.00	0.04	0.50	0.39
5.40	2.50	1.00	0.83	4.00	0.04	0.40	0.33
6.15	3.25	1.00	0.87	4.00	0.04	0.31	0.27
6.90	4.00	1.00	0.89	4.00	0.04	0.25	0.22
4.40	1.50	1.25	0.76	4.48	0.04	0.83	0.51
4.90	2.00	1.25	0.88	4.48	0.04	0.63	0.44
5.40	2.50	1.25	1.01	4.48	0.04	0.50	0.40
6.15	3.25	1.25	1.07	4.48	0.04	0.38	0.33
6.90	4.00	1.25	1.10	4.48	0.04	0.31	0.28
4.40	1.50	1.50	0.78	4.90	0.04	1.00	0.52
4.90	2.00	1.50	0.93	4.90	0.04	0.75	0.47
5.40	2.50	1.50	1.09	4.90	0.04	0.60	0.44
6.15	3.25	1.50	1.25	4.90	0.04	0.46	0.38
6.90	4.00	1.50	1.31	4.90	0.04	0.38	0.33
4.40	1.50	1.75	0.80	5.30	0.04	1.17	0.53
4.90	2.00	1.75	1.02	5.30	0.04	0.88	0.51
5.40	2.50	1.75	1.18	5.30	0.04	0.70	0.47
6.15	3.25	1.75	1.42	5.30	0.04	0.54	0.44
6.90	4.00	1.75	1.50	5.30	0.04	0.44	0.38
4.40	1.50	2.00	0.83	5.66	0.04	1.33	0.55
4.90	2.00	2.00	1.05	5.66	0.04	1.00	0.53
5.40	2.50	2.00	1.28	5.66	0.04	0.80	0.51
6.15	3.25	2.00	1.52	5.66	0.04	0.62	0.47
6.90	4.00	2.00	1.62	5.66	0.04	0.50	0.41

TABLE E.1: Model input for $\frac{H_s}{h_k}$ runs

F $\hat{u}_{33\%}$ near-bed orbital velocities

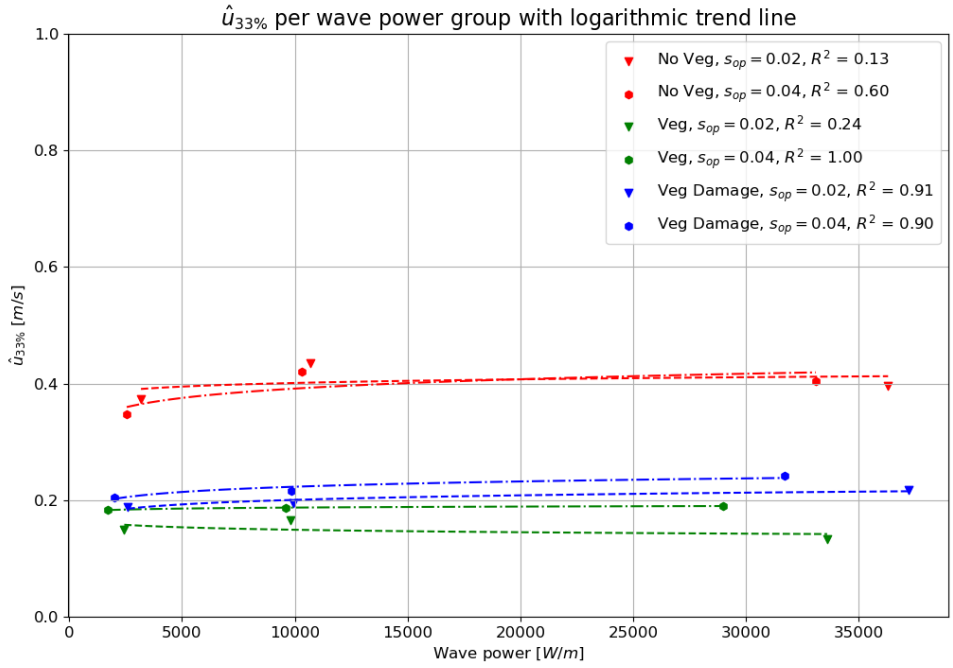

FIGURE F.1: $\hat{u}_{33\%}$ per wave power group, with and without vegetation

G Energy density spectra of numerical modeling

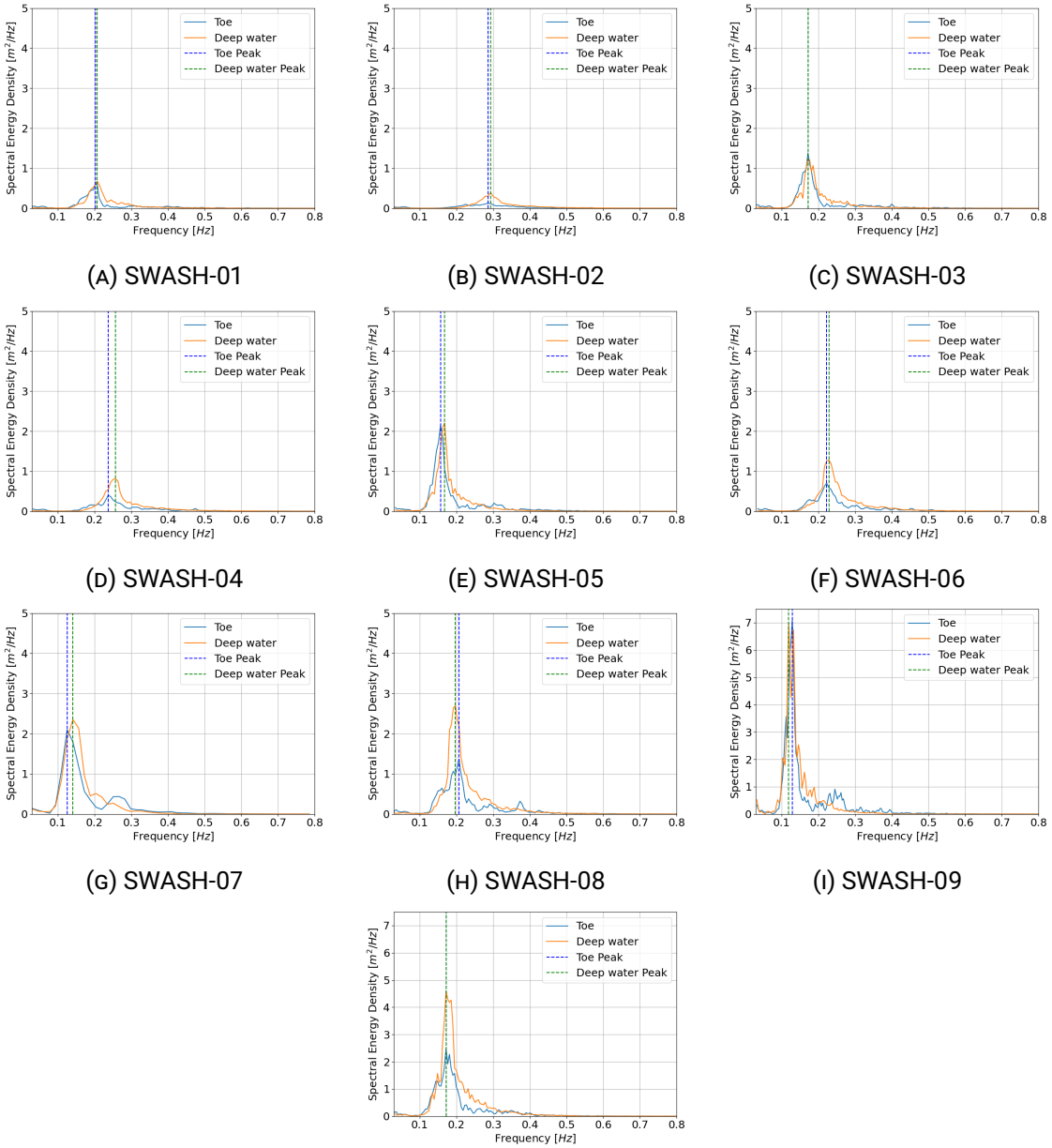

(A) SWASH-01 (B) SWASH-02 (C) SWASH-03

(D) SWASH-04 (E) SWASH-05 (F) SWASH-06

(G) SWASH-07 (H) SWASH-08 (I) SWASH-09

(J) SWASH-10

FIGURE G.1: Spectral plots of all the initial SWASH-model runs

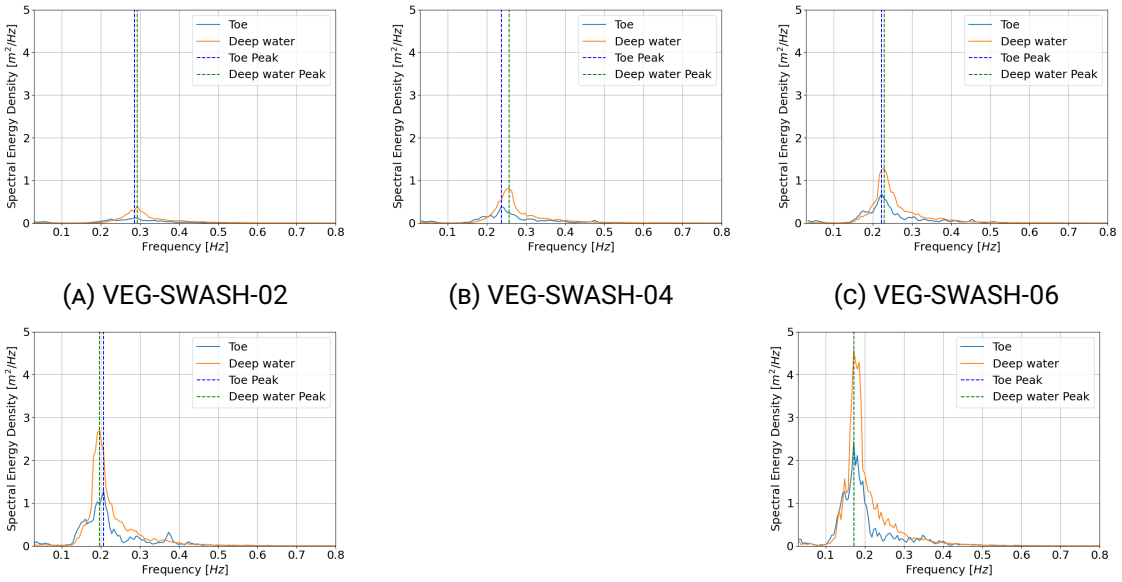

(A) VEG-SWASH-02 (B) VEG-SWASH-04 (C) VEG-SWASH-06

(D) VEG-SWASH-08 (E) VEG-SWASH-10

FIGURE G.2: Spectral plots of all the SWASH-model runs with vegetation